

1 **CRISPR-targeted display of functional T cell receptors enables**
2 **engineering of enhanced specificity and prediction of cross-reactivity**

3

4 Rodrigo Vazquez-Lombardi¹, Johanna S. Jung, Florian Bieberich, Edo Kapetanovic, Erik Aznauryan,
5 Cédric R. Weber and Sai T. Reddy¹

6

7 Department of Biosystems Science and Engineering, ETH Zurich

8 Mattenstrasse 26, 4058 Basel, Switzerland

9 ¹To whom correspondence should be addressed

10 rodrigva@ethz.ch, sai.reddy@ethz.ch

11

12 **ABSTRACT**

13 **T cell receptor (TCR) gene therapy is a promising cell therapy approach for the treatment of cancer.**
14 **However, most naturally occurring TCRs display low affinities to their peptide-MHC targets, and**
15 **engineering of TCRs for enhanced affinity is complicated by the risk of introducing cross-reactivity**
16 **and the poor correlation between affinity and function. Here we report the establishment of the TCR-**
17 **accepting T cell (TnT) platform through five sequential CRISPR-Cas9 genome editing steps of a**
18 **human T cell line, and demonstrate its application for functional engineering of TCRs and prediction**
19 **of cross-reactivity. Using the TnT platform, we profile the mutational landscapes of tumor-specific**
20 **TCRs at high-throughput to reveal a substantial discordance between antigen binding and antigen-**
21 **induced signaling. Furthermore, we combine CRISPR-targeting, functional selection and deep**
22 **sequencing to screen TCR mutagenesis libraries and identify variants with enhanced recognition of**
23 **the cancer-testis antigen MAGE-A3. Finally, functional cross-reactivity profiling using TnT cells was**
24 **able to accurately predict off-targets and identify engineered TCRs with exquisite specificity to**
25 **MAGE-A3. Thus, the TnT platform represents a valuable technology for the engineering of TCRs with**
26 **enhanced functional and safety profiles.**

27 **INTRODUCTION**

28 T cell receptor (TCR) gene therapy is a promising cell therapy approach against cancer that relies on viral
29 transfer of genes encoding the α and β chains of tumor-reactive TCRs into autologous T cells, followed by
30 their expansion and re-infusion into patients¹. Unlike chimeric antigen receptor (CAR)-T cell therapies, which
31 target surface tumor antigens, TCR-redirected T cells recognize processed intracellular tumor antigen
32 peptides displayed by major histocompatibility complex (MHC) / human leukocyte antigen (HLA) molecules.
33 This key feature vastly increases the number of potential antigen targets and is thought to allow for more
34 efficient infiltration into solid tumors², a known limitation of CAR-T cells³. As such, TCR gene therapy has
35 been identified as an effective approach for driving durable responses against multiple cancers^{2,4-12}. Despite
36 its significant promise, the discovery, engineering and selection of optimal therapeutic TCRs remains a time-
37 consuming process complicated by the low affinities of TCRs to their peptide-MHC targets and the inherent
38 risk of TCR cross-reactivity^{6,13,14}.

39 Different from antibodies, which typically recognize a single epitope, TCRs are able to recognize multiple
40 peptide antigens presented by MHC¹⁵. For example, naturally-occurring TCRs have been shown to display
41 a wide range of specificity profiles¹⁶, in some cases having the potential to recognize up to a million different
42 peptides¹⁷. Therefore, cross-reactivity is vital to measure and subsequently avoid in order to engineer safe
43 TCR gene therapies. In addition to specificity, TCR affinity and potency (i.e., functional avidity) are crucial
44 parameters to consider when selecting optimal TCRs for gene therapy applications. Notably, TCR
45 specificity, affinity and function are not necessarily correlated with each other. For example, while TCRs
46 with high affinities to antigen (1-5 μ M) tend to display high potency *in vitro*, TCRs with lower affinities (5-100
47 μ M) often display a poor correlation between affinity and function^{18,19}. In addition, engineered TCRs with
48 supraphysiological affinities (< 1 μ M) may display sub-optimal therapeutic activity due to increased T cell
49 dysfunction^{20,21}, inability to undergo serial TCR triggering²², and potential for reactivity against the presenting
50 HLA molecule^{23,24}.

51

52 Due to central and peripheral negative selection processes, naturally occurring high-affinity TCRs targeting
53 self-antigens are extremely rare and their discovery requires extensive screening²⁵⁻²⁷. To overcome this,
54 directed evolution and protein engineering methods that rely on display technologies (e.g., phage and yeast
55 display) have been employed^{28,29}. These require reformatting of TCRs into synthetic single-chain fragments,
56 which are then screened on the surface of phage or yeast for binding towards peptide-MHC multimers. In
57 one notable example, phage display was used to increase the affinity of a TCR targeting the cancer-testis
58 antigen MAGE-A3. When applied as a TCR gene therapy, unexpected cross-reactivity towards a self-
59 antigen expressed by beating cardiomyocytes cells was observed, which ultimately resulted in treatment-
60 induced patient deaths in a clinical trial^{14,30}. In light of this outcome, the development of TCR display
61 platforms enabling simultaneous TCR engineering and detection of cross-reactivity on the basis of function
62 (i.e., antigen-induced signaling) would be highly desirable. While a number of TCR engineering methods
63 have been developed in mammalian cell lines^{25,31-34} and primary T cells^{35,36}, these have only reported
64 selections based on antigen binding. In addition, their use of viral transduction or plasmid transfection for
65 TCR reconstitution is associated with limitations including random integration, constitutive expression and
66 possible expression of different TCRs by a single cell.

Vazquez-Lombardi et al., CRISPR-targeted display and functional engineering of TCRs

67 Several technologies allowing the assessment of TCR specificity have been reported recently, highlighting
68 a strong interest in the development and safety screening of TCRs for gene therapy. Affinity-based methods
69 include the use of barcoded peptide-MHC multimer libraries for profiling TCRs displayed on primary T
70 cells^{16,37,38} and the assessment of soluble TCR interaction with peptide-MHC libraries displayed on the
71 surface of yeast^{18,39-41}. A potential limitation of such methods, however, is that they are unable to detect
72 very low-affinity interactions between TCR and peptide-MHC that are nevertheless functional⁴². Epitope
73 screening platforms based on cellular function include those relying on the display of peptide libraries by
74 cells expressing chimeric MHC receptors^{43,44}, cells undergoing trogocytosis⁴⁵, or cells harboring reporters
75 of exogenous granzyme activity^{46,47}. Another method for the functional assessment of TCR cross-reactivity
76 involves measuring T cell reactivity to single amino acid mutants of the target peptide, which has been
77 recently utilized to profile the cross-reactivity of phage display-engineered TCRs reformatted for expression
78 in primary T cells^{48,49} or a murine cell line³¹. While all of the above methods focus on specificity screening
79 of TCRs, they have not been reported to directly enable TCR engineering.

80 Here we report the development and application of the TCR-accepting T cell (TnT) platform for the functional
81 display, engineering and cross-reactivity profiling of TCRs. Reconstitution of Jurkat-derived TnT cells with
82 transgenic TCRs was targeted by CRISPR-Cas9 to the endogenous TCR β genomic region, specifically to
83 the recombined complementary determining region 3 β (CDR3 β) sequence, thus providing a monoallelic
84 target that ensured a single integration event in every cell and physiological expression of transgenic TCRs.
85 We use this approach to characterize > 30 individual TCRs and perform functional screening of 437 single
86 amino acid variants and $\sim 150,000$ combinatorial variants. We dissect the mutational landscapes of two
87 TCRs to reveal contrasting patterns and substantial discordance between antigen binding and antigen-
88 induced signalling. Furthermore, through a combination of positive and negative functional selection steps
89 coupled with deep sequencing, we identify combinatorial TCR variants with enhanced recognition of the
90 MAGE-A3 cancer-testis antigen and lacking cross-reactivity to a known off-target peptide. Finally, we use
91 peptide scanning to evaluate the cross-reactivity of resulting engineered TCRs displayed on TnT cells,
92 leading to the identification of TCR variants targeting MAGE-A3 antigen with exquisite specificity and
93 minimal cross-reactivity, which thus represent therapeutic candidates for TCR gene therapy.

94

95 **RESULTS**

96 **Development of a TCR-accepting T cell (TnT) platform for the functional display of transgenic TCRs**
97 The development of the TnT platform required extensive, multistep CRISPR-Cas9 genome editing. Using
98 the human Jurkat E6-1 leukemia T cell line as a starting point, several genomic components were
99 sequentially edited in order to facilitate the introduction and functional screening of TCRs of different
100 specificities (Fig. 1a and Supplementary Fig. 1). Each genome editing step consisted of transfection with a
101 gene-targeting guide RNA (gRNA) and, when required, a homology-directed repair (HDR) template
102 encoding desired transgenes. This was followed by single-cell fluorescence-activated cell sorting (FACS),
103 cell expansion and clone validation by flow cytometry and Sanger sequencing. In the first step, we equipped
104 the Jurkat T cell line with constitutive Cas9 and human CD8 expression by CRISPR-Cas9 HDR targeting
105 the CCR5 safe harbor locus⁵⁰ (Supplementary Figs. 2a-e). This was performed in order to simplify and
106 increase genome editing efficiency⁵¹, and to allow screening of CD8+ T cell-derived TCRs recognizing MHC
107 class I-restricted peptides. In line with this, in the second step we knocked out the endogenous Jurkat CD4

Vazquez-Lombardi et al., CRISPR-targeted display and functional engineering of TCRs

108 co-receptor by CRISPR-Cas9 non-homologous end joining (NHEJ) (Supplementary Figs. 3a-c). In the third
109 step, we introduced an NFAT-GFP construct into the AAVS1 safe harbor locus through CRISPR-Cas9 HDR,
110 which provides a fluorescence reporter of TCR signaling and activation (Supplementary Figs. 4a-e). Notably,
111 our design incorporated a promoter-less mRuby cassette that acted as a PPP1R12C gene-trap⁵² and served
112 to identify successfully edited cells. In the fourth step, we targeted the endogenous Jurkat TCR α chain for
113 knockout through CRISPR-Cas9 NHEJ, leading to the generation of a cell line with abolished surface
114 expression of the TCR-CD3 complex (Supplementary Figs. 5a-f). In addition to eliminating the possibility of
115 transgenic TCR chains mispairing with the endogenous Jurkat TCR α chain, this approach allows us to use
116 restoration of CD3 surface expression as a selectable marker for successful integration of transgenic TCRs
117 (Figs. 1a-c). In the final step, we knocked out expression of the Fas cell surface death receptor (Fas) by
118 CRISPR-Cas9 NHEJ in order to provide our platform with resistance to activation-induced cell death (AICD)
119 (Supplementary Figs. 6a-c). This resulting cell line constitutively expresses Cas9, human CD8 and mRuby,
120 harbors an NFAT-GFP reporter of TCR signaling, and lacks expression of CD4, endogenous TCR and Fas,
121 and thus represents the TnT platform used throughout the rest of this study.
122

123 We next reconstituted TnT cells with transgenic TCRs in a manner that would allow for monoallelic,
124 homogenous and physiological TCR expression. To this end, we used CRISPR-Cas9 HDR to target
125 integration of TCR transgenes to the recombined Jurkat TCR β locus. First, we confirmed that the Jurkat T
126 cell line expresses a single TCR β chain by performing template-switching RT-PCR and Sanger sequencing
127 (Supplementary Figs. 7a-b). We then designed and validated a gRNA molecule targeting the CDR3 β of the
128 Jurkat TCR β chain (Supplementary Fig. 7c). Since the CDR3 β sequence arises from the allele-independent
129 recombination of V-, D- and J-genes, it provides a genomic target that is both highly specific and monoallelic.
130 Having identified a suitable gRNA, we then proceeded to design TCR β HDR templates for targeted TCR
131 reconstitution in TnT cells. We selected three previously discovered TCRs recognizing HLA-A*0201-
132 restricted tumor-associated antigens: TCR_{1G4} with specificity to NY-ESO-1, and TCR_{DMF4} and TCR_{DMF5} with
133 specificity to MART-1⁵³ (Supplementary Table 1). HDR templates contained sequences encoding TCR α
134 variable (VJ α) and constant (TRAC) domains, a self-processing T2A peptide and a TCR β variable (VDJ β)
135 domain, flanked by ~ 900 bp homology arms mapping to the recombined Jurkat TCR β locus (Fig. 1b). The
136 lack of a constant TCR β domain (TRBC) in the designed constructs made splicing with endogenous Jurkat
137 TRBC exons a requirement for transgenic TCR expression. This feature allowed us to detect targeted
138 genomic integration based on restored surface expression of CD3 following transfection of TnT cells with
139 CDR3 β gRNA and designed HDR templates (PCR product) (Fig. 1c). Furthermore, our strategy ensured
140 that cells displaying restored CD3 expression underwent knockout of the endogenous Jurkat TCR β chain,
141 as integration of transgenic TCRs relied on the introduction of a dsDNA break at the targeted CDR3 β
142 genomic region. Although our initial experiments yielded HDR efficiencies of 1-2%, the development of an
143 enhanced transfection protocol led to HDR efficiencies in the range of 5-20% (Fig. 3c and Supplementary
144 Fig. 8). Targeted TCR reconstitution for the generation of TnT-TCR cells was further validated by detecting
145 binding to cognate peptide-MHC dextramer using flow cytometry (Fig. 1d), PCR amplification of the Jurkat
146 TCR genomic locus (Fig. 1e) and RT-PCR using reverse primers annealing to endogenous Jurkat TRBC
147 sequences (Supplementary Figs. 9a and 9b). We thus successfully generated TnT-TCR_{1G4}, TnT-TCR_{DMF4}
148 and TnT-TCR_{DMF5} cell lines that were then subjected to further functional validation.

Vazquez-Lombardi et al., CRISPR-targeted display and functional engineering of TCRs

149

150 In order to assess antigen-induced signaling in TnT-TCR cells, we performed co-culture experiments using
151 the HLA-A*0201-positive T2 cell line⁵⁴. Co-culture of TnT-TCR_{1G4} cells with unpulsed (no peptide) T2 cells
152 yielded no detectable expression of NFAT-GFP, while co-culture with T2 cells pulsed with NY-ESO-1₁₅₇₋₁₆₅
153 cognate peptide induced robust expression of the NFAT-GFP reporter (Fig. 1f). To further assess the
154 specificity of our platform, we performed co-cultures of TnT, TnT-TCR_{1G4}, TnT-TCR_{DMF4} and TnT-TCR_{DMF5}
155 cells with T2 cells pulsed with NY-ESO-1₁₅₇₋₁₆₅ peptide, MART-1_{26-35(2L)} peptide or no peptide. We found that
156 NFAT-GFP expression was fully restricted to correct TCR-peptide pairings, with no detectable NFAT-GFP
157 expression across negative controls (Fig. 1g).

158

159 We next compared the binding and functional avidities of TnT-TCR_{1G4}, TnT-TCR_{DMF4} and TnT-TCR_{DMF5} cells
160 (Fig. 1h-i). TnT-TCR_{DMF5} cells displayed the highest binding avidity to their target peptide-MHC (EC50 = 7
161 pM), followed by TnT-TCR_{1G4} (EC50 = 57 pM) and TnT-TCR_{DMF4} (EC50 = 267 pM), with picomolar EC50
162 values reflecting the multivalent nature of surface-displayed TCRs and peptide-MHC dextramers (10-20
163 peptide-MHC copies per molecule). We evaluated the functional avidity of TnT-TCR cells following co-
164 culture with T2 cells pulsed with serial dilutions of cognate peptide, which revealed a dose-dependent
165 response in terms of NFAT-GFP-expressing cells (Fig. 1i). TnT-TCR_{DMF5} displayed the highest functional
166 avidity (EC50 = 6 nM), followed by TnT-TCR_{DMF4} (EC50 = 11 nM) and TnT-TCR_{1G4} (EC50 = 90 nM). In
167 contrast to their 39-fold difference in binding to peptide-MHC dextramer, the difference between TnT-
168 TCR_{DMF4} and TnT-TCR_{DMF5} in terms of functional avidity was only 2-fold. This indicated that a high binding
169 avidity is not a requirement for antigen-induced expression of NFAT-GFP in TnT-TCR cells. Finally,
170 additional co-culture experiments confirmed TnT-TCR resistance to AICD (Supplementary Fig. 6d) and
171 physiological down-regulation of surface TCR-CD3 expression with increasing amounts of presented
172 antigen⁵⁶ (Supplementary Fig. 6e).

173

174 **Deep mutational scanning reveals the expression, binding and functional landscapes of TCRs**

175 In contrast to previous TCR engineering methods^{28,29}, the TnT platform allows us to assess TCRs across
176 multiple parameters which include their surface expression in complex with CD3, binding to peptide-MHC
177 multimers and signaling in response to antigen-presentation. We selected the MART-1-specific TCR_{DMF4}
178 and the MAGE-A3-specific TCR_{A3} for comprehensive profiling using the TnT platform (Fig. 2a). TCR_{A3} is a
179 low-avidity TCR isolated from a melanoma patient treated with a viral vaccine encoding the HLA-A*0101-
180 restricted MAGE-A3₁₆₈₋₁₇₆ peptide^{57,58} (Supplementary Table 1). Co-culture experiments with the MAGE-A3-
181 positive EJM myeloma cell line revealed that the avidity of TCR_{A3} was not sufficient to induce NFAT-GFP
182 expression in TnT-TCR_{A3} cells. However, we detected increased surface expression of the early T cell
183 activation marker CD69 following co-culture, which provided us with a complementary and more sensitive
184 functional readout (Supplementary Fig. 10c).

185

186 Having characterized parental TCR_{DMF4} (Fig. 1g-i) and TCR_{A3}, we aimed to determine their mutational
187 landscapes across the multiple parameters provided by TnT cells. To this end, we performed deep
188 mutational scanning (DMS) of CDR3 β as this TCR region is typically enriched for direct contacts to peptide
189 antigen rather than to MHC⁵⁵. To generate DMS libraries we introduced NNK degenerate codons at each

Vazquez-Lombardi et al., CRISPR-targeted display and functional engineering of TCRs

190 CDR3 β position using plasmid nicking saturation mutagenesis⁵⁹ (Supplementary Figs. 11a-c). Plasmid DMS
191 libraries were then used to generate TCR $\alpha\beta$ HDR templates (PCR products), which were transfected into
192 TnT cells alongside CDR3 β gRNA (Supplementary Fig. 11b). TnT cells displaying restored TCR-CD3
193 surface expression were isolated by FACS (SEL 1), expanded and re-sorted based on binding to cognate
194 peptide-MHC dextramer (SEL 2A) or activation following co-culture with cells displaying target peptides
195 (SEL 2B) (Fig. 2b and Supplementary Figs. 12a-c). Due to the low avidity of the parental TCR $_{A3}$, functional
196 selections of TCR $_{A3}$ DMS libraries were based on CD69 expression, instead of NFAT-GFP. Following FACS,
197 deep sequencing was performed to identify TCR variants that were enriched across selection steps.

198

199 Sequence enrichment analysis was performed relative to observed variant frequencies in plasmid DMS
200 libraries of TCR $_{A3}$ (Fig. 2c) and TCR $_{DMF4}$ (Fig. 2d). We found that wild-type TCR sequences (Figs. 2c and
201 2d, boxed residues) were enriched in most selections, which likely reflected the depletion of unfavorable
202 variants. The only exception occurred in TCR $_{A3}$ SEL 2B (signaling), in which wild-type TCR $_{A3}$ was depleted
203 relative to the original plasmid library. This was in agreement with the low levels of antigen-induced signaling
204 found in TnT-TCR $_{A3}$ cells (Supplementary Fig. 12c), and pointed towards the occurrence of TCR $_{A3}$ single
205 mutants with substantial increases in function relative to wild-type TCR $_{A3}$. In terms of TCR-CD3 expression
206 (SEL 1), we detected sequencing reads originating from all but five TCR $_{A3}$ variants, indicating that the vast
207 majority of TCR $_{A3}$ mutants were capable of cell surface expression in complex with CD3 (Fig. 2c). This was
208 in stark contrast to the TCR $_{DMF4}$ surface expression landscape, which was heavily restricted (Fig. 2d). As
209 expected, the mutational landscapes for peptide-MHC binding (SEL 2A) and antigen-induced signaling (SEL
210 2B) were more restricted than those seen for TCR-CD3 surface expression (Figs. 2c and 2d). In the case
211 of TCR $_{A3}$, while a similar number of enriched variants was observed in binding (SEL 2A) and signaling (SEL
212 2B) selections, there was little correlation between the deep sequencing enrichment levels of individual
213 variants in the two fractions (Fig. 2c and Supplementary Fig. 13a). Some TCR $_{A3}$ variants, however, did
214 display high levels of sequence enrichment for both parameters (e.g., S3G, P4L, M6L and A7V)
215 (Supplementary Fig. 13a). In the case of TCR $_{DMF4}$, there was a modest correlation between enrichment
216 levels of individual variants in binding (SEL 2A) and signaling (SEL 2B) fractions (Supplementary Fig. 13b).
217 However, a very limited number of TCR $_{DMF4}$ variants displayed enrichment levels that were higher than wild-
218 type TCR $_{DMF4}$ for either binding or signaling. Notably, the number of enriched TCR $_{DMF4}$ variants in the
219 signaling fraction (SEL 2B) was considerably higher than in the binding fraction (SEL 2A). This indicated
220 that antigen-induced signaling may occur in the absence of detectable peptide-MHC binding in some of
221 these TCR $_{DMF4}$ variants, particularly those with substitutions in CDR3 β positions 2-4 (Fig. 2d).

222

223 In order to further characterize the discordance observed between antigen binding and antigen-induced
224 signaling, we reconstituted TnT cells with variants showing enrichment above wild-type TCR levels. For
225 TCR $_{A3}$, we selected nine variants (S3G, P4F, P4L, P4M, P4T, N5C, M6L, A7V, Q10Y) and included the
226 high-affinity TCR $_{A3a}$ as a positive control (see next section for more information on TCR $_{A3a}$). For TCR $_{DMF4}$,
227 we selected six variants (I2H, I2L, E4F, E4Q, E4P, E4V) and included the high-affinity TCR $_{DMF5}$ as a positive
228 control. All selected TCR variants were successfully expressed on the surface of TnT cells and were
229 assessed for binding with cognate peptide-MHC dextramer (Fig. 2e, g top row) and antigen-induced
230 signaling (Fig. 2e, g bottom row). Notably, the majority of TCR $_{A3}$ variants displayed enhancements in binding

Vazquez-Lombardi et al., CRISPR-targeted display and functional engineering of TCRs

231 and signaling relative to wild-type TCR_{A3}. Consistent with sequence enrichment data, variants S3G, P4L,
232 M6L and A7V displayed the largest increases in terms of both binding and signaling (Fig. 2f). For TCR_{DMF4}
233 variants, only modest improvements were observed relative to wild-type (Fig. 2i), namely enhanced binding
234 of variants I2L, E4V and E4F to MART-1 peptide-MHC dextramer (Fig. 2 h). Surprisingly, TCR_{DMF4} variants
235 I2H and I2L showed similar levels of antigen-induced signaling despite I2H showing no detectable binding
236 to MART-1 peptide-MHC dextramer (Figs. 2g and 2h), further highlighting the discordance between binding
237 and signaling in certain TCRs.

238

239 **Functional selection of combinatorial CDR3 β libraries identifies TCRs with enhanced target
240 specificity and reactivity**

241 Next, we aimed to engineer the low-avidity TCR_{A3} for enhanced reactivity to the cancer-testis antigen MAGE-
242 A3, as it represents an attractive target that is widely expressed in several types of epithelial tumors⁶⁰. In a
243 previous effort, TCR_{A3} was engineered by phage display to generate TCR_{a3a}, a variant with >200-fold higher
244 affinity to MAGE-A3₁₆₈₋₁₇₆ peptide-MHC^{14,30} (Supplementary Fig. 10a and Supplementary Table 1).
245 However, use of TCR_{a3a} in a gene therapy clinical trial resulted in two treatment-induced patient deaths¹⁴.
246 Retrospective analysis uncovered that TCR_{a3a} cross-reactivity to a peptide derived from the protein titin,
247 which is highly expressed in beating cardiomyocytes, led to fatal cardiac toxicity³⁰. Notably, this occurred
248 despite the titin-derived peptide (ESDPIVAQY) having four amino acid differences relative to MAGE-A3<sub>168-
249 176</sub> (EVDPIGHLY). Consistent with previous findings, we found that TnT-TCR_{A3} cells showed low but
250 detectable binding and TnT-TCR_{a3a} showed high binding to MAGE-A3 peptide-MHC dextramer, while only
251 TnT-TCR_{a3a} displayed binding to titin peptide-MHC dextramer (Supplementary Fig. 10b).

252

253 We sought to generate and screen combinatorial CDR3 β libraries using the TnT platform in order to identify
254 TCR variants with enhanced antigen specificity and reactivity. Combinatorial library design was based on
255 data obtained from TCR_{A3} DMS (Fig. 2c), as this allowed us to maximize both library functionality and size
256 for screening in mammalian cells⁵¹. By utilizing a sequence space optimization algorithm⁵¹, we designed
257 degenerate codons that mimic the TCR_{A3} single mutant frequencies found in DMS binding and signaling
258 selections (Supplementary Fig. 14), leading to a combinatorial library diversity of 2.6×10^5 (Fig. 3a). The
259 designed TCR_{A3} combinatorial library was generated by overlap-extension PCR, and cloned into a TCR_{A3-}
260 encoding plasmid for bacterial transformation (Supplementary Fig. 15a). We estimated that the physical
261 plasmid library contained as many as 1.5×10^5 TCR_{A3} variants based on the number of bacterial
262 transformants and the proportion of unique clones after deep sequencing (Supplementary Fig. 15b). The
263 constructed TCR_{A3} plasmid library was used to generate HDR templates, which were then integrated into
264 TnT cells by CRISPR-Cas9 HDR.

265

266 The selection strategy for the TnT-TCR_{A3} library consisted of a combination of positive and negative
267 selection steps based on binding to peptide-MHC dextramers and signaling in response to cell-displayed
268 antigens, with deep sequencing of TCR regions performed after every selection step (Fig. 3b). In the first
269 selection step, TnT cells displaying restored CD3 expression were isolated by FACS and expanded (SEL
270 1, Fig. 3c). Next, expanded cells from SEL 1 were co-cultured overnight with MAGE-A3-positive EJM cells
271 and co-stained with MAGE-A3 and titin peptide-MHC dextramers. Different to wild-type TnT-TCR_{A3} cells, a
272 fraction of TnT-TCR_{A3} library cells displayed robust NFAT-GFP expression (Fig. 3d). Analysis of the NFAT-

Vazquez-Lombardi et al., CRISPR-targeted display and functional engineering of TCRs

273 GFP-positive population revealed that ~ 20% of cells that bound to MAGE-A3 also recognized the titin
274 peptide-MHC dextramer (Fig. 3d). In order to exclude these cross-reactive variants, we isolated cells that
275 were NFAT-GFP-positive, MAGE-A3 peptide-MHC dextramer-positive and titin peptide-MHC dextramer-
276 negative (SEL 2). A final functional selection step was performed by co-culturing expanded cells from SEL
277 2 with Colo 205 cells pulsed with either MAGE-A3 or titin peptides. As expected, we observed a substantial
278 fraction of TnT-TCR cells with NFAT-GFP expression after co-culture with MAGE-A3-pulsed Colo 205 cells
279 (Fig. 3e). Interestingly, we also found that a subset of TnT-TCR cells still expressed NFAT-GFP in response
280 to titin stimulation despite the exclusion of titin peptide-MHC binders in SEL 2. Analysis of the sequence
281 space landscape revealed a number of notable trends, including the preference of alanine codons at position
282 CDR3 β -1 for TCR:CD3 expression (SEL 1), and the increased frequency of specific residues at CDR3 β -6
283 and CDR3 β -10 in MAGE-A3-based selections (SEL 2 and SEL 3A). Most notably, we observed a substantial
284 increase in the frequency of glutamate residues at CDR3 β -6 in SEL 3B (titin-induced signaling), highlighting
285 this substitution as a potential determinant of titin cross-reactivity.

286
287 We next analyzed deep sequencing data for clone enrichment (Supplementary Table 2). We identified a
288 total of 195 unique clones displaying greater than 2-fold enrichment in SEL 3A (MAGE-A3 signaling) and
289 that were either absent or not enriched in SEL 3B (titin signaling). We scored these clones based on their
290 frequency and enrichment levels and identified the top 29 candidate TCR_{A3} variants, of which we selected
291 14 for further characterization (Fig. 3g and Supplementary Table 3). To this end, we reconstituted TnT cells
292 with wild-type TCR_{A3}, TCR_{a3a} and selected TCR_{A3} variants via CRISPR-Cas9 HDR and assessed them for
293 CD3 expression, binding to MAGE-A3 and titin peptide-MHC dextramers. All selected TCR_{A3} variants were
294 successfully displayed on the surface of TnT cells and showed enhanced MAGE-A3 dextramer binding
295 relative to wild-type TnT-TCR_{A3} cells (Fig 3h). Importantly, binding to titin peptide-MHC dextramer was
296 undetectable in most of the selected TCR_{A3} variants, while readily detected in TnT cells displaying the phage
297 display-engineered TCR_{a3a} (Fig 3i).

298
299 **The TnT platform enables TCR cross-reactivity profiling and accurate prediction of off-target
300 antigens**

301 Since engineering TCRs for enhanced reactivity carries the risk of introducing unwanted specificities, we
302 decided to apply the TnT platform for the screening of TCR cross-reactivity. As a proof of concept, we
303 profiled the cross-reactivity of the phage display-engineered TCR_{a3a}³⁰, which has titin as a known off-target,
304 by performing deep mutational scanning (DMS) of the MAGE-A3 target peptide. Accordingly, we designed
305 a synthetic peptide DMS library containing every possible single amino acid mutant of MAGE-A3₁₆₈₋₁₇₆
306 (EVDPIGHLY) (n = 171). Each library peptide was then individually pulsed on Colo 205 cells (HLA-A*0101-
307 positive, MAGE-A3-negative) and co-cultured with TnT-TCR_{a3a} cells (n = 171 co-cultures). Activation of TnT-
308 TCR_{a3a} cells was assessed by NFAT-GFP expression, which was corrected for background and normalized
309 to the response induced by Colo 205 cells pulsed with wild-type MAGE-A3 peptide (Fig. 4a). In agreement
310 with a previous glycine-serine scan³⁰, we found that most mutations at peptide-MHC positions 1, 3, 4, 5 and
311 9 of the target MAGE-A3 peptide resulted in substantially reduced TnT-TCR_{a3a} activation. By contrast,
312 several peptides with mutations at positions 2, 6, 7 and 8 induced strong activation of TnT-TCR_{a3a} cells.

313

Vazquez-Lombardi et al., CRISPR-targeted display and functional engineering of TCRs

314 In order to predict potential off-targets, we generated peptide sequence space motifs of allowed substitutions
315 at discrete thresholds of TnT-TCR_{a3a} activation, and used them to interrogate the UniProtKB database^{48,49}.
316 As expected, the number of unique peptide hits resulting from these searches decreased with increasing
317 activation thresholds (Fig. 4b), as this reflected the use of more restricted peptide motifs (Supplementary
318 Table 4). The only human peptide returned at the highest activation threshold (100%) was indeed the target
319 MAGE-A3₁₆₈₋₁₇₆ (EVDPIGHLY) (Fig. 4b). Remarkably, the human peptide returned at the second highest
320 activation threshold was the titin peptide ESDPIVAQY, which was identified despite the fact that the most
321 similar peptides in the DMS library had three amino acid mismatches. The human peptide returned at the
322 third highest activation threshold was MAGE-A6₁₆₈₋₁₇₆ (EVDPIGHVY), another known target of TCR_{a3a}³⁰. We
323 also identified the cancer-testis antigen MAGE-B18₁₆₆₋₁₇₄ (EVDPIRHYY), which has been previously shown
324 to activate TCR_{a3a}³⁰.

325

326 We next selected a subset of predicted off-target peptides with potential clinical relevance for experimental
327 validation. These were peptides returned across several activation thresholds and included ten human and
328 two viral peptides (Supplementary Table 5). We also included the bacterial *C. difficile* EKDPIKENY peptide,
329 which was predicted in a previous study to be a potential off-target of TCR_{a3a}³⁰, but was not predicted in our
330 high-resolution DMS analysis as inclusion of lysine at position 2 resulted in negligible TnT-TCR_{a3a} activation
331 (Fig. 4a). Peptides were pulsed on Colo 205 cells and co-cultured with TnT-TCR_{a3a} cells overnight, followed
332 by assessment of activation based on both NFAT-GFP and CD69 expression. MAGE-A3 induced strong
333 expression of NFAT-GFP and CD69, while MAGE-A6 and MAGE-B18 also induced substantial but lower
334 activation (Fig. 4c). Since NFAT-GFP expression was low in some co-cultures, quantification of CD69^{high}
335 TnT-TCR_{a3a} cells allowed us to identify peptides inducing responses significantly higher than background
336 (CMV negative control peptide) (Fig. 4d). We found that titin significantly activated TnT-TCR_{a3a} cells,
337 however this response was still considerably lower than that induced by MAGE-A3, which is consistent with
338 the reported 50-fold difference in the binding affinity of TCR_{a3a} towards titin peptide-MHC³⁰. We also found
339 that human peptides derived from the proteins ANR16, CD166 and MRCKA isoform 2; and a peptide derived
340 from a Kaposi Sarcoma-associated herpesvirus exonuclease (AN_HHV8P) induced significant activation of
341 TnT-TCR_{a3a} cells (Fig. 4d), and thus represent potentially novel and clinically relevant off-targets of TCR_{a3a}.
342

343 Having profiled TCR_{a3a} cross-reactivity through target peptide DMS, we wondered if any of the resulting off-
344 targets were capable of activating our engineered TCR_{A3} combinatorial variants (Fig. 3g-i). To assess this
345 possibility, we co-cultured TnT cells expressing wild-type TCR_{A3}, TCR_{a3a} or selected TCR_{A3} variants with
346 Colo 205 cells pulsed with activating off-target peptides (excluding MAGE-A6 and MAGE-B18), as well as
347 MAGE-A3, titin and CMV control peptides (Fig. 4e). We found that all TnT-TCR_{A3} variants displayed a
348 stronger response to MAGE-A3 than wild-type TnT-TCR_{A3}, which showed negligible activation. Interestingly,
349 we found that TnT -TCR_{A3-27} and TnT-TCR_{A3-28} were activated by titin. While the low response observed in
350 TnT-TCR_{A3-28} cells might be explained by its residual level of binding to titin peptide-MHC dextramer (Fig.
351 3i), the robust response in TnT-TCR_{A3-27} cells was highly unexpected considering its minimal binding to titin
352 peptide-MHC dextramer (Fig. 3i). In contrast, TnT-TCR_{A3-09} showed higher binding to titin peptide-MHC
353 dextramer than TnT-TCR_{A3-27} cells (Fig 3i) but were not activated in response to titin-induced signaling (Fig
354 5e and Supplementary Fig. 15). These results provide further examples of the discordance between TCR

Vazquez-Lombardi et al., CRISPR-targeted display and functional engineering of TCRs

355 antigen binding and signaling, and emphasize the importance of functional screening to better assess TCR
356 specificity and cross-reactivity. Another interesting finding was that negative selection against titin
357 recognition (Figs. 3b and 3c) did not impede the emergence of additional cross-reactivity to other peptides
358 in some of the engineered TCR_{A3} variants. This was clearly the case for variants TCR_{A3-09} (cross-reactive to
359 ANR16 and MRCKA) and TCR_{A3-12} (cross-reactive to CD166 and MRCKA), which provide examples of
360 increased cross-reactivity following TCR engineering (Fig. 4e). Most importantly, we found that variants
361 TCR_{A3-03}, TCR_{A3-04}, TCR_{A3-05}, TCR_{A3-08} and TCR_{A3-10} showed low or negligible activation in response to all
362 tested peptides (Fig. 4e, highlighted in blue, and Supplementary Fig. 17).

363

364 **Engineered TCRs expressed in primary human T cells display high target reactivity with minimal**
365 **cross-reactivity**

366 As a final validation step, we profiled the activities of selected engineered TnT-TCR_{A3} variants in primary
367 human CD8+ T cells. To achieve this, we adapted a CRISPR-Cas9-based method for dual knockout of
368 endogenous TCR α and TCR β chains and simultaneous reconstitution with transgenic TCRs targeted to the
369 TRAC locus^{56,61,62} (Fig. 5a). The lack of a complete TRAC region in the designed TCR β a HDR templates
370 made splicing with endogenous TRAC exons a requirement for transgenic TCR surface expression. In order
371 to confirm targeted TCR reconstitution, we first validated this approach using TCR_{a3a}. Accordingly, RT-PCR
372 using a forward TRBV5-1 (present in TCR_{a3a}) primer and reverse endogenous TRAC primer yielded a 1.6
373 kb product only in T cells transfected with both gRNA and HDR template (Fig. 5b). Sanger sequencing of
374 the resulting product revealed correct integration of TCR_{a3a} sequences. By contrast, a control RT-PCR
375 amplification of TCR α chains utilizing the TRAV21 gene yielded products of expected size for test and
376 control transfections (Fig. 5b). Flow cytometry confirmed CD3 expression and binding to MAGE-A3 peptide-
377 MHC dextramer in T cells reconstituted with TCR_{a3a}, and a greater than 95% endogenous TCR knockout
378 efficiency (Fig. 5c).

379

380 We next generated primary human CD8+ T cells expressing wild-type TCR_{A3}, TCR_{a3a}, selected TCR_{A3}
381 variants or no transgenic TCR (TCR KO). In order to verify transgenic TCR function, we first co-cultured
382 transfected T cells with MAGE-A3-positive EJM or MAGE-A3-negative Colo205 cells, and assessed their
383 activation by means of IFN- γ ELISpot (Figs. 5d and 5e). No significant differences in MAGE-A3-induced
384 activation were observed in T cells transfected with wild-type TCR_{A3}, TCR_{A3-04}, or no TCR (Fig. 5e). Notably,
385 while wild-type TCR_{A3} showed a minimal response to EJM cells, the complete lack of response observed in
386 T cells transfected with TCR_{A3-04} indicated that this variant was not successfully expressed by primary T
387 cells. In contrast, we found that T cells expressing TCR_{a3a}, TCR_{A3-03}, TCR_{A3-05}, TCR_{A3-08} and TCR_{A3-10} were
388 strongly and significantly activated after co-culture with EJM cells (Figs. 5d and 5e).

389

390 We next performed a series of co-culture experiments using peptide-pulsed Colo 205 cells (HLA-A*0101-
391 positive, MAGE-A3-negative) coupled with IFN- γ ELISpot readouts. Consistent with our results using TnT-
392 TCR cells, we observed TCR_{a3a} cross-reactivity to titin, while titin-induced responses in our engineered
393 TCR_{A3} variants were either absent or of lower magnitude (Fig. 5f and Supplementary Fig. 18). Notably,
394 primary T cells expressing TCR_{a3a} showed a significant titin-induced IFN- γ response relative to background,
395 with a magnitude that was 62% of their observed MAGE-A3 response (Fig. 5f). We also observed a low but

Vazquez-Lombardi et al., CRISPR-targeted display and functional engineering of TCRs

396 significant titin-induced IFN- γ response in primary T cells expressing TCR_{A3-08} (Fig. 5f). Importantly, we
397 found that primary T cells expressing variants TCR_{A3-03}, TCR_{A3-05} or TCR_{A3-10} displayed a significant MAGE-
398 A3-induced IFN- γ response but undetectable activation following co-culture with titin-pulsed Colo 205 cells
399 (Fig. 5f). Furthermore, primary T cells expressing wild-type TCR_{A3} showed a similarly negligible titin-induced
400 response in this assay (Fig. 5f). Assessment of TCR cross-reactivity against off-target peptides previously
401 identified for TCR_{a3a} revealed that primary T cells expressing TCR_{A3-03} or TCR_{A3-08} had significant IFN- γ
402 responses to peptides derived from CD166, MRCKA isoform 2 and AN_HHV8 (TCR_{A3-08} only), and were
403 thus excluded from further characterization (Supplementary Fig. 19). By contrast, primary T cells expressing
404 TCR_{A3-05} or TCR_{A3-10} displayed high levels of specificity for the MAGE-A3 target peptide, with no other
405 peptide inducing detectable responses.

406

407 Given the remarkable specificity of variants TCR_{A3-05} and TCR_{A3-10}, we next decided to assess their cross-
408 reactivity profiles using the TnT platform and DMS of the target MAGE-A3₁₆₈₋₁₇₆ peptide (EVDPIGHLY). We
409 assessed activation of TnT-TCR cells by flow cytometric detection of CD69 expression, as we previously
410 validated it as a more sensitive readout for cross-reactivity detection (Fig. 4c). Similar to TnT-TCR_{a3a} peptide
411 DMS (Fig. 4a), most mutations at positions 1, 3, 4, 5 and 9 were detrimental for TnT-TCR_{A3-05} and TnT-
412 TCR_{A3-010} activation (Figs. 5g-h). Remarkably, we found that several peptides with mutations at positions 6
413 and 7, which were mostly activating in TnT-TCR_{a3a} cells, led to substantially reduced activation in TnT-
414 TCR_{A3-10} and TnT-TCR_{A3-05} cells. Of note, we found that the presence of valine at peptide position 6, a
415 substitution present in the titin off-target peptide (ESDPIV~~A~~QY), drastically reduced responses in both TnT-
416 TCR_{A3-05} and TCR_{A3-10} (4-8% of the wild-type MAGE-A3 response), which rationalizes the lack of cross-
417 reactivity of these engineered TCR_{A3} variants to titin (Fig. 5f). As a way of comparison, the same peptide
418 induced a response of 91% relative to wild-type MAGE-A3 in TnT-TCR_{a3a} cells (Fig. 4a).

419

420 Querying of the UniProtKB database with motifs derived from peptide DMS data of TnT-TCR_{A3-05} and TnT-
421 TCR_{A3-10} revealed substantial reductions in the number of predicted off-targets relative to TnT-TCR_{a3a}, both
422 in terms of human and non-human sequences (Fig. 5i and Supplementary Fig. 20). Most notably, the MAGE-
423 A3 target peptide became the only returned human hit for TCR_{A3-05} and TCR_{A3-10} at much lower activation
424 thresholds (26% and 44%, respectively) than TCR_{a3a} (89%), further highlighting their reduced tolerance to
425 peptide substitutions. In a similar manner, additional human hits for TCR_{A3-05} and TCR_{A3-10} were returned at
426 considerably lower activation thresholds relative to TCR_{a3a} (Fig. 5j).

427

428 DISCUSSION

429 Here we describe the development of the TnT platform, an extensively CRISPR-edited human T cell line
430 that supports the functional display, engineering and cross-reactivity profiling of TCRs. TnT cells harbor
431 fully-defined genomic changes that facilitate the display and functional engineering of transgenic TCRs at
432 high-throughput. As such, the TnT platform provides important advantages over previous TCR engineering
433 methods that rely exclusively on affinity-based readouts, especially in light of the poor correlation that exists
434 between TCR affinity and function^{18,19}. Furthermore, TCR reconstitution by CRISPR-Cas9 targeting of the
435 endogenous TCR β locus offers several advantages over plasmid transfection³³ or viral transduction^{25,31,32,34-}
436 ³⁶ such as homogenous and physiological expression of TCRs, and occurrence of a single integration event

Vazquez-Lombardi et al., CRISPR-targeted display and functional engineering of TCRs

437 per cell ensured by targeting of the monoallelic Jurkat CDR3 β genomic sequence. Furthermore, optimization
438 of our CRISPR-Cas9 HDR protocol led to TCR integration efficiencies of up to 20%, which allowed for the
439 screening of large mutagenesis libraries and selection of variants with enhanced specificity and function.
440

441 The unique features of the TnT platform allowed us to apply CDR3 β DMS to comprehensively profile two
442 tumor-reactive TCRs (TCR_{A3} and TCR_{DMF4}) for their patterns of expression, antigen binding and antigen-
443 induced signaling. Deep sequencing of original libraries and FACS selections was a crucial component of
444 our TCR engineering pipeline (both in DMS and combinatorial selections) as it allowed us to accurately
445 determine the enrichment of specific TCR variants across selections. Remarkably, we identified several
446 variants that were enriched for antigen binding but not for antigen-induced signaling, and vice-versa, which
447 emphasized the discordance between TCR binding and function. For example, two TCR_{DMF4} variants had
448 nearly identical signaling capacity despite one of them displaying undetectable binding to the MART-1
449 peptide-MHC dextramer. This is in agreement with previous reports of peptide-MHC multimers failing to
450 detect fully functional TCRs⁴². Crucially, DMS enrichment data allowed us to tailor the design of a
451 combinatorial TCR_{A3} library in order to maximize the number of productive variants.
452

453 We utilized the TnT platform for engineering the MAGE-A3-specific TCR_{A3}, a naturally occurring low-avidity
454 TCR that has been previously engineered by phage display, which resulted in affinity-enhanced variants
455 with cross-reactivity to titin^{14,30,63}. To this end, we designed a DMS-based combinatorial library of CDR3 β
456 TCR_{A3} and used the TnT platform to perform selections based on binding and signaling in response to both
457 MAGE-A3 and titin antigens. Throughout the selection process, we observed the emergence of TCR_{A3}
458 variants with enhanced binding and signaling in response to MAGE-A3. Interestingly, we found that a
459 considerable proportion of library members also displayed binding and signaling in response to titin,
460 highlighting the high propensity of TCR_{A3} mutants to develop titin cross-reactivity. By using deep sequencing
461 enrichment data, we could identify TCR_{A3} variants with increased binding and function in response to MAGE-
462 A3 that neither bound or responded to titin. Surprisingly, we found that some variants (e.g., TCR_{A3-27} and
463 TCR_{A3-28}) displayed robust signaling in response to titin, despite showing low or undetectable binding to titin-
464 MHC dextramer. This finding further emphasizes the importance of functional screening of engineered
465 TCRs, as screening approaches based on binding alone may fail to identify cross-reactive TCRs^{16,40}.
466 Remarkably, TCR_{A3-05}, which showed the highest specificity to MAGE-A3 throughout our experiments in
467 both TnT cells and primary T cells, was the variant with the highest score for predicted MAGE-A3 specificity
468 based on deep sequencing enrichment data (Supplementary Table 3). Taken together, these findings
469 highlight the power of TnT functional selections coupled with deep sequencing for engineering highly specific
470 TCRs.
471

472 The TnT platform allows us to both engineer TCRs and assess their cross-reactivity potential without the
473 need of reformatting TCRs for cellular display^{31,48,49} or soluble expression^{39,40}. By performing DMS of the
474 target MAGE-A3₁₆₈₋₁₇₆ peptide, we predicted and validated known and potentially novel off-targets for
475 TCR_{A3a}. Despite its four amino acid difference to MAGE-A3, the titin ESDPIVAQY peptide was identified at
476 the second highest activation threshold. Interestingly, we also identified a peptide derived from MRCKA
477 isoform 2 (UniProtKB, Q5VT25-2) as a potential TCR_{A3a} off-target, and confirmed its ability to activate TnT-

Vazquez-Lombardi et al., CRISPR-targeted display and functional engineering of TCRs

478 TCR_{a3a} cells *in vitro*. As MRCKA is highly expressed in the heart⁶⁴, it is possible that recognition of this
479 peptide may have also contributed to the cardiac toxicity elicited by TCR_{a3a}¹⁴. We observed that a number
480 of our engineered TCR_{A3} variants were activated by predicted TCR_{a3a} off-targets. As these TnT-TCR_{A3}
481 variants showed weaker binding to MAGE-A3 peptide-MHC than TnT-TCR_{a3a} (TCR_{a3a} K_D ~ 2.3 – 6.6
482 μM)^{23,30}, they constitute examples of cross-reactivity emergence in engineered TCRs within the
483 physiological affinity range (1 – 100 μM)¹⁹.

484

485 Assessment of primary T cell activation by means of IFN- γ ELISpot assays showed a higher sensitivity than
486 CD69 expression in TnT-TCR cells following co-culture, which may reflect higher levels of co-receptors in
487 primary CD8+ T cells relative to TnT cells. Despite this difference, we were able to identify variants that
488 displayed remarkable specificity for MAGE-A3, namely TCR_{A3-05} and TCR_{A3-10}, in both TnT-TCR and primary
489 T cell assays. Functional cross-reactivity profiling of these variants using the TnT platform revealed a large
490 reduction in the number of predicted off-targets compared to TCR_{a3a}. While reduced cross-reactivity was
491 particularly evident for titin, it was also observed for peptides that were not negatively selected for (e.g.,
492 MAGE-A6, CD166 and MRCKA isoform 2), thus highlighting TCR_{A3-05} and TCR_{A3-10} as intrinsically specific
493 variants. This is consistent with the recent identification of naturally-occurring TCRs displaying a wide range
494 of specificity levels for the same target¹⁶. Thus, the enhanced function and specificity of TCR_{A3-05} and TCR_{A3-10}
495 make them promising candidates for use in TCR gene therapies targeting MAGE-A3-positive tumors in
496 HLA-A*0101-positive patients. Thus, the ability of the TnT platform to support both TCR engineering and
497 the accurate prediction of cross-reactivity on the basis of function makes it a promising technology for the
498 development of therapeutic TCRs with improved efficacy and safety profiles.

499 **METHODS**

500 **Cell lines and cell culture**

501 The Jurkat leukemia E6-1 T cell line was obtained from the American Type Culture Collection (ATCC)
502 (#TIB152); the T2 hybrid cell line (#ACC598) and the EJM multiple myeloma cell line (#ACC560) were
503 obtained from the German Collection of Cell Culture and microorganisms (DSMZ); and the Colo 205 colon
504 adenocarcinoma cell line (#87061208) was obtained from the European Collection of Authenticated Cell
505 Cultures (ECACC). Jurkat cells, engineered TnT cells and Colo 205 cells were cultured in ATCC-modified
506 RPMI-1640 (Thermo Fisher, #A1049101), T2 cells were cultured in RPMI-1640 (Thermo Fisher,
507 #11875093), and EJM cells were cultured in IMDM (Thermo Fisher, #12440053). All media were
508 supplemented with 10% FBS, 50 U ml⁻¹ penicillin and 50 µg ml⁻¹ streptomycin. Detachment of EJM and Colo
509 205 adherent cell lines for passaging was performed using the TrypLE reagent (Thermo Fisher, #12605010).
510 All cell lines were cultured at 37 °C, 5% CO₂ in a humidified atmosphere.

511

512 **Polymerase chain reaction (PCR)**

513 PCRs for cloning, generation of HDR templates, genotyping of mammalian cells, generation of TCR libraries
514 and generation of amplicons for deep sequencing were performed using the KAPA HiFi PCR kit with GC
515 buffer (Roche Diagnostics, #07958846001) and custom designed primers (Supplementary Table 6).
516 Annealing temperatures (x) were optimized for each reaction by gradient PCR and cycling conditions were
517 as follows: 95°C for 3 min; 35 cycles of 98°C for 20 s, x°C for 15 s, 72°C for 30 s per kb; final extension
518 72°C for 1 min per kb. PCRs for genotyping of bacterial colonies after transformation were performed using
519 the KAPA2G Fast ReadyMix kit (Sigma Aldrich, #KK5102) with custom designed primers and the following
520 cycling conditions: 95°C for 3 min; 35 cycles of 95°C for 15 s, 60°C for 15 s, 72°C for 15 s per kb; final
521 extension 72°C for 1 min per kb.

522

523 **Cloning and generation of HDR templates**

524 DNA for gene-encoding regions and homology regions were generated by gene synthesis (Twist
525 Bioscience) or PCR and introduced into desired plasmid backbones via restriction cloning (Supplementary
526 File 1). The following plasmids were used as backbones: pX458 (Addgene, #48138),
527 AAVS1_Puro_Tet3G_3xFLAG_Twin_Strep (Addgene, #92099), pGL4.30 (Promega, #E8481) and pTwist
528 Amp High Copy (Twist Bioscience). Targeted knock-in of Cas9/GFP into the CCR5 locus was performed
529 utilizing circular plasmid DNA as the HDR template. HDR templates for all other targeted knock-in
530 experiments were provided as linear double-stranded DNA (dsDNA) generated by PCR. Prior to
531 transfection, PCR products were column-purified using the QIAquick PCR Purification Kit (Qiagen, #28106).
532 For targeted TCR reconstitution of TnT cells, homology arms flanking the recombined Jurkat TCRβ VDJ
533 locus were designed and cloned in pTwist (Twist Bioscience), resulting in pJurTCRB. TCRαβ cassettes
534 encoding transgenic TCRs were generated by gene synthesis (Twist Bioscience) and cloned into pJurTCRB
535 using naturally-occurring XbaI and BsaI restriction sites present within the homology arms. Next, HDR
536 templates were generated by PCR using primer pair RVL-127/128 and PCR products purified prior to
537 transfection. For targeted TCR reconstitution of primary human CD8+ T cells, TCRβα cassettes lacking
538 TRAC exons 2-3 and flanked by homology arms mapping to TRAC exon 1⁵⁶ were designed and cloned in

Vazquez-Lombardi et al., CRISPR-targeted display and functional engineering of TCRs

539 pTwist (Twist Bioscience). HDR templates were generated by PCR using primer pair RVL-164/165 and PCR
540 products purified prior to transfection.

541

542 **CRISPR-Cas9 genome editing**

543 Transfection of TnT cells and Jurkat-derived cell lines was performed by electroporation using the 4D-
544 Nucleofector device (Lonza) and the SE cell line kit (Lonza, #V4XC-1024). The day before transfection, cells
545 were seeded at 2.5×10^5 cells/mL and cultured for 24 h. Prior to transfection, gRNA molecules
546 (Supplementary Table 7) were assembled by mixing 4 μ L of custom Alt-R crRNA (200 μ M, IDT) with 4 μ L of
547 Alt-R tracrRNA (200 μ M, IDT, #1072534), incubating the mix at 95°C for 5 min and cooling it to room
548 temperature. For transfection of Cas9-negative cell lines, 2 μ L of assembled gRNA molecules were mixed
549 with 2 μ L of recombinant SpCas9 (61 μ M, IDT, #1081059) and incubated for > 10 min at room temperature
550 to generate Cas9 RNP complexes. Immediately prior to transfection, cells were washed twice in PBS and
551 1×10^6 cells were re-suspended in 100 μ L of SE buffer. 1.5 μ g of HDR template and 7 μ L of assembled gRNA
552 (or 4 μ L of Cas9 RNP complexes) were added to the cell suspension, mixed and transferred into a 1 mL
553 electroporation cuvette. Cells were electroporated using program CK116, topped-up with 1 mL of complete
554 media and rested for 10 min prior to transfer into a 12-well plate. Alt-R HDR enhancer (IDT, #1081073) was
555 added at a 30 μ M final concentration and removed after 16 h of culture by centrifugation. HDR efficiency
556 was assessed by flow cytometry on day 5 post-transfection. For transfections at the 20 μ L scale (Lonza,
557 #V4XC-1032), cell numbers and reagent volumes were reduced 5-fold.

558

559 **Flow cytometry and fluorescence-activated cell sorting (FACS)**

560 Flow cytometric analysis of cell lines and primary T cells was performed according to standard protocols.
561 The following antibodies were purchased from BioLegend and used at 1 μ g ml^{-1} in flow cytometry buffer
562 (PBS, 2% FBS, 2 mM EDTA): PE-Cy7-conjugated or APC-conjugated anti-human CD3e (clone UCHT1,
563 #300420 or #300458), APC-conjugated anti-human CD4 (clone RPA-T4, #300552), PE-conjugated anti-
564 human CD8a (clone HIT8a, #300908), PE-Cy7-conjugated anti-human CD19 (clone HIB19, #302216), APC-
565 conjugated anti-human CD69 (clone FN50, #310910), APC-conjugated anti-human Fas (clone DX2,
566 #305611) and PE-conjugated anti-human TCR α/β (clone IP26, #306707). DAPI viability dye (Thermo
567 Fisher, #62248) was added to antibody cocktails at a final concentration of 1 μ g ml^{-1} . Cells were washed
568 once in flow cytometry buffer prior to staining, stained for 20 min on ice and washed twice in flow cytometry
569 buffer before analysis using BD LSRIFortessa or Beckman-Coulter CytoFLEX flow cytometers. Blocking of
570 Fc receptors in T2 cells was performed prior to staining using the TruStain FcX reagent (BioLegend,
571 #422301). Staining with peptide-MHC dextramers was performed for 10 min at room temperature (RT),
572 followed by addition of 2X antibody cocktails (2 μ g ml^{-1} antibodies, 2 μ g ml^{-1} DAPI) and incubation for 20
573 min on ice. The following peptide-MHC dextramers were commercially obtained from Immudex: NY-ESO-
574 1₁₅₇₋₁₆₅ (SLLMWITQC, HLA-A*0201, #WB2696-APC); MART-1_{26-35(27L)} (ELAGIGILTV, HLA-A*0201,
575 #WB2162-APC); MAGE-A3₁₆₈₋₁₇₆ (EVDPIGHLY, HLA-A*0101, #WA3249-PE) and titin_{24,337-24,345}
576 (ESDPIVAQY, HLA-A*0101, custom-made, APC-conjugated). Peptide-MHC dextramers were used at a 3.2
577 nM final concentration (i.e., 1:10 dilution) for staining, unless indicated otherwise in figure legends. FACS
578 was performed using BD FACSaria III or BD FACSaria Fusion instruments. Single-cell sorts were collected

Vazquez-Lombardi et al., CRISPR-targeted display and functional engineering of TCRs

579 in 96-well flat-bottom plates containing conditioned media and clones were cultured for 2-3 weeks prior to
580 characterization.

581

582 **Genotyping of cell lines and transfectants**

583 Genomic DNA was extracted from 2×10^5 cells by resuspension in 100 μ L of QuickExtract solution (Lucigen,
584 #0905T), incubation at 65°C for 6 min, vortexing for 15 s and incubation at 98°C for 2 min. 5 μ L of genomic
585 DNA extract were then used as templates for 25 μ L PCR reactions. For genotyping by two-step reverse
586 transcription PCR (RT-PCR), RNA from 1×10^5 cells was extracted using the TRIZol reagent (Invitrogen, #
587 15596018) and column-purified using the PureLink RNA Mini kit (Invitrogen, #12183025). For reverse
588 transcription, 100 pmol of oligo dT, 10 nmol of each dNTP, 5 μ L RNA and sufficient nuclease-free water for
589 a final 14 μ L volume were mixed, incubated at 65°C for 5 min and chilled on ice for 5 min. This was followed
590 by addition of 4 μ L of 5X RT buffer, 40 units of RiboLock RNase inhibitor (Thermo Fisher, #EO0381) and
591 200 units of Maxima H-minus reverse transcriptase (Thermo Fisher, #EP0751) and mixing. In some
592 experiments, 40 pmol of template-switching oligonucleotide (TSO, Supplementary Table 6) was added for
593 labelling of first-strand cDNA 3' ends⁶⁵. Reverse transcription was performed at 50°C for 30 min, followed
594 by inactivation at 85°C for 5 min. 5 μ L of the resulting cDNA-containing reverse transcription mixes were then
595 used as templates for 25 μ L PCR reactions.

596

597 **Peptides and peptide pulse**

598 Peptides and peptide libraries were generated by custom peptide synthesis (Genscript), re-suspended at
599 10 μ g ml^{-1} in DMSO and placed at -80°C for prolonged storage. For peptide pulsing, T2 cells or Colo 205
600 cells were harvested and washed twice in serum-free RPMI 1640 (SF-RPMI). Peptides were diluted to 10
601 μ g ml^{-1} in SF-RPMI (or to concentrations indicated in figure legends) and the solution was used to re-
602 suspend cells at 1×10^6 cells ml^{-1} . Cells were incubated for 90 min at 37°C, 5% CO₂, washed once with SF-
603 RPMI, re-suspended in complete media and added to co-culture wells (see section below).

604

605 **TnT stimulation and co-culture assays**

606 For clone screening and assessment of AICD, TnT cells and Jurkat-derived cell lines were stimulated
607 overnight with either 10 μ g ml^{-1} plate-bound anti-human CD3e antibody (clone OKT3, BioLegend, #317326)
608 or 1X eBioscience Cell Stimulation Cocktail (81 nM PMA, 1.34 μ M ionomycin; Thermo Fisher, #00497093).
609 For co-culture experiments, TnT-TCR cells at $\sim 1 \times 10^6$ cells ml^{-1} density were harvested, pelleted by
610 centrifugation and re-suspended in fresh complete media at 1×10^6 cells ml^{-1} . 1×10^5 TnT-TCR cells (100 μ L)
611 were seeded in wells of a V-bottom 96-well plate. Antigen-expressing cells (EJM) or peptide-pulsed cells
612 (T2, Colo 205) were adjusted to 1×10^6 cells ml^{-1} in complete media and 5×10^4 cells (50 μ L) added to each
613 well. Anti-human CD28 antibody (clone CD28.2, BioLegend, #302933) was added at a final concentration
614 of 1 μ g ml^{-1} for co-stimulation of all samples (including negative controls) and plates were incubated
615 overnight at 37°C, 5% CO₂. The next day, expression of NFAT-GFP and CD69 in TnT-TCR cells was
616 assessed by flow cytometry. Flow cytometric discrimination between TnT-TCR cells and Colo 205 cells (or
617 EJM cells) was based on side scatter area (SSC-A) and mRuby expression, while discrimination between
618 TnT-TCR cells (CD19-negative) and T2 cells (CD19-positive) was based on CD19 expression.

619

Vazquez-Lombardi et al., CRISPR-targeted display and functional engineering of TCRs

620 **Generation of deep mutational scanning (DMS) libraries**

621 DMS libraries of the CDR3 β regions of TCR $_{A3}$ and TCR $_{DMF4}$ were generated by plasmid nicking mutagenesis
622 as described in Wrenbeck et al. 2016⁵⁹. The protocol relies on the presence of a single BbvCI restriction site
623 for sequential targeting with Nt.BbvCI and Nb.BbvCI nickases, digestion of wild-type plasmid and plasmid
624 re-synthesis using mutagenic oligonucleotides. A plus-strand BbvCI restriction site was introduced into the
625 pJurTCRB-TCR $_{A3}$ plasmid by means of PCR and blunt-end ligation, while the endogenous minus-strand
626 BbvCI site present in the TRBV10-3 gene of pJutTCRB-TCR $_{DMF4}$ was targeted. The order of BbvCI nickase
627 digestion was adjusted for each plasmid so that the plus DNA strand was digested first. Mutagenic
628 oligonucleotides were designed using the QuikChange Primer Design online tool (Agilent) and assessed for
629 the presence of secondary structures using the Oligo Evaluator online tool (Sigma-Aldrich) (Supplementary
630 Table 6). Oligonucleotides showing strong potential for forming secondary structures were manually
631 modified to reduce this propensity. After nicking mutagenesis, mutated plasmids were transformed into 100
632 μ L of chemically-competent *E. coli* DH5 α cells (NEB, #C2987H) and plated on ampicillin (100 μ g ml $^{-1}$) LB
633 agar in Nunc BioAssay dishes (Sigma-Aldrich, #D4803). Serial dilutions of transformed cells were plated
634 separately to quantify bacterial transformants. Plasmid libraries were purified from bacterial transformants
635 using the QIAprep Spin Miniprep kit (Qiagen, #27106). HDR templates were generated from plasmid
636 libraries by PCR using primer pair RVL-127/128 and column-purified prior to transfection.
637

638 **DMS library screening and selections**

639 DMS library HDR templates and CDR3B gRNA were used to transfect 1x10 6 TnT cells. In TCR $_{A3}$ DMS
640 selections, cells with restored CD3 surface expression and no binding to control titin peptide-MHC dextramer
641 were isolated by FACS on day 8 post-transfection (SEL 1). Sorted cells were expanded for 13 days and
642 either stained with MAGE-A3 peptide-MHC dextramer or co-cultured overnight with MAGE-A3-positive EJM
643 cells. Dextramer-positive cells (SEL 2A) and activated CD69 high cells (SEL 2B) were then isolated by FACS.
644 In TCR $_{DMF4}$ DMS selections, cells with restored CD3 surface expression and no binding to control NY-ESO-
645 1 peptide-MHC dextramer were isolated by FACS on day 8 post-transfection (SEL 1). Sorted cells were
646 expanded for 13 days and either stained with MART-1 peptide-MHC dextramer or co-cultured overnight with
647 MART-1 peptide-pulsed T2 cells. Dextramer-positive cells (SEL 2A) and activated NFAT-GFP-positive cells
648 (SEL 2B) were then isolated by FACS.
649

650 **Generation of combinatorial TCR $_{A3}$ libraries**

651 Degenerate codons reflecting the combined CDR3 β amino acid frequencies observed in TCR $_{A3}$ DMS
652 binding and signaling selections (SEL2A+2B) were determined as previously described⁵¹. The library
653 resulting from two iterations of our algorithm was modified to include VNB codons at CDR3 β positions 4 and
654 6. For library construction, ssDNA oligonucleotides containing a 28 nt complementary overlap were
655 designed and purchased as custom ultramers (IDT, Supplementary Table 6). The forward ultramer encoded
656 exclusively wild-type TCR $_{A3}$ codons, while the reverse ultramer contained the reverse complement of both
657 wild-type and library degenerate codons. 200 pmol of each ultramer were mixed and subjected to single-
658 cycle PCR using the following conditions: 95°C for 3 min, 98°C for 20 s, 70°C for 15 s, 72°C for 10 min. The
659 resulting 270 bp dsDNA product was gel-purified (Zymogen, #D4002) and 8 ng were utilized as template for
660 a 200 μ L PCR reaction using external primers with the following cycling conditions: 95°C for 3 min; 25 cycles

Vazquez-Lombardi et al., CRISPR-targeted display and functional engineering of TCRs

661 of 98°C for 20 s, 62°C for 15 s, 72°C for 15 s; final extension 72°C for 30 s. The PCR product was column-
662 purified, digested with KpnI and Bsal restriction enzymes, and re-purified. In parallel, the pJurTCRB-TCRA3
663 plasmid was digested with KpnI and Bsal, de-phoshorylated (CIP, NEB, #M0290) and gel-purified. Digested
664 PCR product (112.5 ng) and plasmid (750 ng) were ligated in a 75 μ l reaction containing 1X T4 PNK buffer,
665 1 mM ATP and 3 units of T4 DNA ligase for 2 h at RT (all from NEB). Next, the ligation mix was transformed
666 into 750 μ L of chemically-competent *E. coli* DH5 α cells (NEB, #C2987I) and plated on ampicillin LB agar in
667 Nunc BioAssay dishes. Quantification of bacterial transformants, purification of plasmid library and
668 generation of HDR templates was performed as described for DMS libraries.

669

670 **Combinatorial TCR_{A3} library screening and selections**

671 Combinatorial library HDR templates (20 μ g) and CDR3B gRNA (10 nmol) were used to transfect 1x10⁸ TnT
672 cells using the 4D-Nucleofector LV unit (Lonza, #AAF-1002L). TnT cells with restored CD3 surface
673 expression were bulk-sorted (SEL 1) on day 6 post transfection. SEL 1 cells were expanded for 6 days prior
674 to overnight co-culture with MAGE-A3-positive EJM cells followed by co-staining with MAGE-A3 and titin
675 peptide-MHC dextramers. After co-culture, NFAT-GFP-positive cells displaying positive MAGE-A3 peptide-
676 MHC binding and negative titin peptide-MHC binding were bulk-sorted (SEL 2) and expanded in culture for
677 12 days. SEL 2 cells were co-cultured overnight with either peptide MAGE-A3-pulsed (MAGE-A3) or titin-
678 pulsed Colo 205 cells. Activated NFAT-GFP-positive cells from MAGE-A3 (SEL 3A) and titin (SEL 3B) co-
679 cultures were bulk-sorted for RNA extraction, RT-PCR and deep sequencing.

680

681 **Deep sequencing and analysis of TCR libraries**

682 TCR amplicons for deep sequencing of plasmid libraries were generated by PCR using primer pair RVL-
683 144/154, while TCR amplicons for deep sequencing of TnT-TCR selections were generated by two-step RT-
684 PCR using primer pair RVL-144/145. In both cases, PCR was limited to 25 cycles. TCR amplicons were
685 column-purified and deep-sequenced using the Amplicon-EZ service (Genewiz), which includes
686 adaptor/index ligation and paired-end Illumina sequencing (250 cycles) followed by delivery of 50,000
687 assembled reads per sample with unique sequence identification and abundance analysis. For DMS plasmid
688 libraries and selections, unique sequences with less than ten sequencing reads were excluded from
689 enrichment analysis, as every library member had sequencing reads above this threshold. Sequence
690 enrichment of unique DMS variants was determined by dividing their observed frequencies in SEL 1 (TCR-
691 CD3 expression), SEL 2A (binding) and SEL 2B (signaling) over their plasmid DMS library frequencies, and
692 heatmaps were generated using the GraphPad Prism software. For the TCR_{A3} combinatorial plasmid library
693 and selections, unique clone frequency data was filtered to remove clones containing insertions, deletions
694 or mutations outside CDR3 β . Filtered data was used to generate sequence logos weighted on amino acid
695 frequencies at specific CDR3 β positions using R packages ggseqlogo⁶⁶ and ggplot2. The frequencies of
696 specific TCR_{A3} variants across selections were identified by merging unique clone datasets using a custom
697 Python script. Sequence enrichment of unique TCR_{A3} combinatorial variants was determined by dividing
698 their observed frequencies in SEL 2 (MAGE-A3-induced activation and binding), SEL 3A (MAGE-A3-
699 induced activation) and SEL 3B (titin-induced activation) over their SEL 1 (TCR-CD3 expression)
700 frequencies.

701

Vazquez-Lombardi et al., CRISPR-targeted display and functional engineering of TCRs

702 **Peptide DMS and assessment of TCR cross-reactivity**

703 A DMS library of the target MAGE-A3₁₆₈₋₁₇₆ EVDPIGHLY peptide was designed and generated by custom
704 peptide synthesis (Genscript). Each library member (n = 171) was individually pulsed at a 50 μ g ml⁻¹
705 concentration on Colo 205 cells for co-culture with TnT-TCR cells (n = 171 co-cultures). Co-cultures with
706 MAGE-A3-pulsed (n = 3), titin-pulsed (n = 3), CMV-pulsed (n = 6) peptides and unpulsed (n = 6) Colo 205
707 cells were included as controls. After overnight co-culture, TnT-TCR activation was assessed by NFAT-GFP
708 and CD69 expression by means of flow cytometry. The mean background activation observed in CMV
709 peptide controls (i.e., VTEHDTLLY peptide pulse) was subtracted from all samples and their responses
710 normalized to the mean MAGE-A3 response level. Normalized data was used to generate heatmaps
711 (GraphPad Prism), weighted sequence logos (ggseqplot, ggplot2 in R) and peptide sequence motifs of
712 allowed substitutions at discrete activation thresholds (Bioconductor package Biostrings in R). Peptide
713 sequence motifs (Supplementary Table 4) were then used to query the UniProtKB database (including splice
714 variants) with the ScanProsite online tool. The output of these searches was processed using the Biostrings
715 package in order to compute the number of unique peptide hits.

716

717 **Primary T cell culture and genome editing**

718 Human peripheral blood mononuclear cells were purchased from Stemcell Technologies (#70025) and
719 CD8+ T cells isolated using the EasySep Human CD8+ T Cell Isolation kit (Stemcell Technologies, #17953).
720 Primary human CD8+ T cells were cultured for up to 24 days in ATCC-modified RPMI (Thermo Fisher,
721 #A1049101) supplemented with 10% FBS, 10 mM non-essential amino acids, 50 μ M 2-mercaptoethanol,
722 50 U ml⁻¹ penicillin, 50 μ g ml⁻¹ streptomycin and freshly added 20 ng ml⁻¹ recombinant human IL-2-
723 (Peprotech, #200-02). T cells were activated with anti-CD3/anti-CD28 tetrameric antibody complexes
724 (Stemcell Technologies, #10971) on days 1 and 13 of culture and expanded every 3-4 days. Transfection
725 of primary T cells with Cas9 RNP complexes and TCR β α HDR templates was performed 3-4 days following
726 activation using the 4D-Nucleofector and a 20 μ L format P3 Primary Cell kit (Lonza, V4XP-3032). Briefly,
727 1x10⁶ primary CD8+ T cells were transfected with 1 μ g of HDR template, 1 μ l of TRAC Cas9 RNP complex
728 and 1 μ l of TRBC1/2 Cas9 RNP complex using the EO115 electroporation program (Cas9 RNP complexes
729 = 50 μ M gRNA, 30.5 μ M recombinant SpCas9). For RT-PCR validation of TCR reconstitution, RNA was
730 extracted from 1x10⁶ T cells, quantified using a Nanodrop instrument, and 40 ng RNA used as input for
731 reverse transcription. 2 μ L of reverse transcription mixes were then utilized as templates for 25 μ L PCR
732 reactions.

733

734 **Co-culture of primary T cells and IFN- γ ELISpot**

735 IFN- γ ELISpot assays were performed using the Human IFN- γ ELISpot Pair (BD, #551873), 96-well ELISpot
736 plates (Millipore, #MSIPS4W10), Avidin-HRP (Biolegend, #405103) and precipitating TMB substrate
737 (Mabtech, #3651-10). Wells were activated with 15% (v/v) ethanol for 30 s, washed twice with PBS and
738 coated with 5 μ g ml⁻¹ capture antibody (in PBS) at 4°C overnight (or up to a week). On the day of co-culture
739 (i.e., day 5 post-transfection), wells were washed twice with PBS and blocked with primary T cell media
740 lacking IL-2 (RP10-TC) for > 2 h at 37°C. In parallel, TCR-reconstituted primary CD8+ T cells were rested
741 in the absence IL-2 for 6 h. After resting, T cells were washed and re-suspended in fresh RP10-TC media.
742 A 100 μ L volume of cell suspensions containing 5x10⁴ to 4x10⁵ T cells was then transferred into blocked

Vazquez-Lombardi et al., CRISPR-targeted display and functional engineering of TCRs

743 ELISpot wells, as specified in figure legends. Next, 1.5×10^4 antigen-expressing (EJM) or peptide-pulsed
744 (Colo 205) cells were added into wells in a 50 μL volume of RP10-TC media. Anti-CD28 monoclonal antibody
745 was added into every well at a $1 \mu\text{g ml}^{-1}$ final concentration and plates were incubated for 20 h at 37°C, 5%
746 CO₂. Following co-culture, cells were removed and wells washed three times with wash buffer (0.01%(v/v)
747 Tween 20 in PBS). Detection antibody was then added at $2 \mu\text{g ml}^{-1}$ in dilution buffer (0.5%(v/v) BSA in PBS)
748 followed by 2 h incubation at RT. After incubation, wells were washed three times with wash buffer and
749 1:2000 avidin-HRP (in dilution buffer) added for 45 min at RT. Wells were washed three times with wash
750 buffer and once in PBS, followed by development with precipitating TMB substrate for 3-10 min at RT.
751 Development was stopped by washing with deionized water and plates were dried for > 24 h in the dark
752 prior to analysis using an AID ELR08 ELISpot reader (Autoimmun Diagnostika).

753

754 **AUTHOR CONTRIBUTIONS**

755 R.V.-L. and S.T.R. designed the study; R.V.-L., J.J. and S.T.R. contributed to experimental design; R.V.-
756 L., J.J., F.B., E.A. and E.K. performed experiments; R.V.-L., J.J., F.B., and C.R.W. analyzed data; R.V.-L.
757 and S.T.R. wrote the manuscript with input from all authors.

758

759 **ACKNOWLEDGMENTS**

760 We thank Dr. Joseph Taft for his advice on the plasmid nicking mutagenesis method, and Darya Palianina
761 for her assistance with ELISpot assays. We acknowledge the ETH Zurich D-BSSE Single Cell Unit for their
762 assistance with FACS. This study is supported by funding from the Personalized Health and Related
763 Technologies Postdoctoral Fellowship (to R.V.-L), the NCCR Molecular Systems Engineering (to S.T.R.)
764 and Helmut Horten Stiftung (to S.T.R.).

765

766 **COMPETING INTERESTS**

767 ETH Zurich has filed for patent protection on the technology described herein, and R.V.-L., J.J. and S.T.R.
768 are named as co-inventors on this patent (European Patent Application: EP19202970.0).

769

770 **DATA AVAILABILITY**

771 The raw FASTQ files from deep sequencing that support the findings of this study will be deposited in the
772 Sequence Read Archive (SRA) with the primary accession code(s) <code(s)>
773 (<https://www.ncbi.nlm.nih.gov/sra>). Additional data that support the findings of this study are available from
774 the corresponding author upon reasonable request.

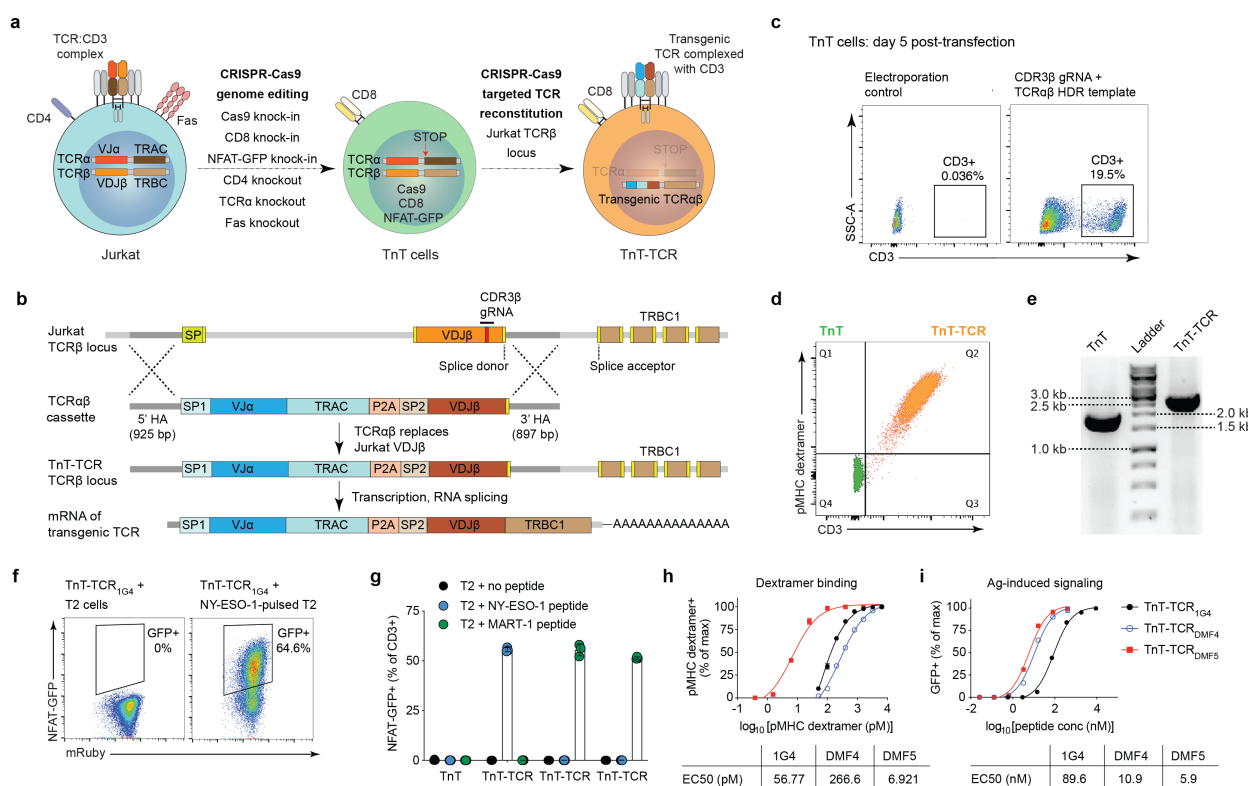
775

776

777

778

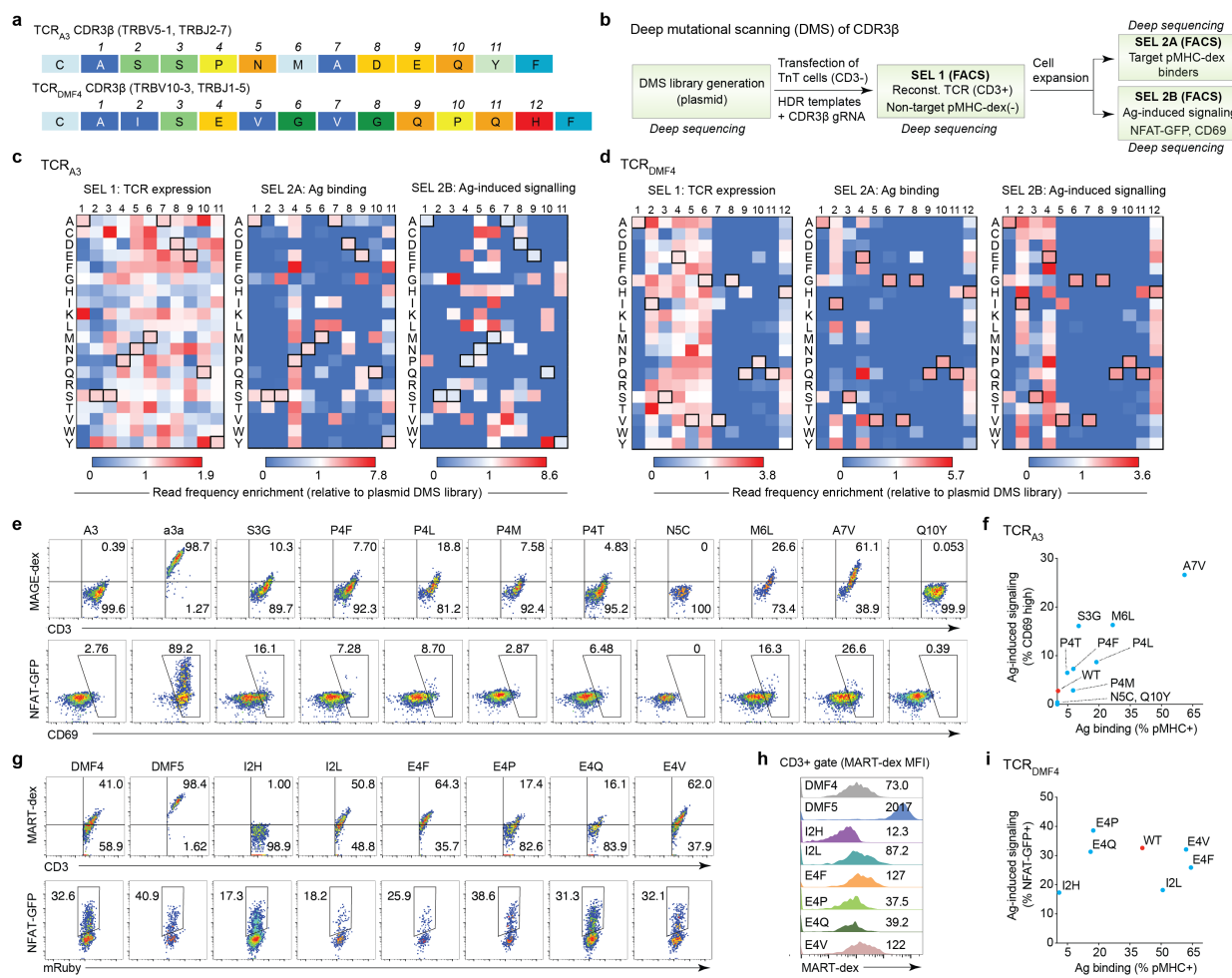
Figure 1_Vazquez-Lombardi et al.



779

Figure 1. The TCR-accepting T cell (TnT) platform supports targeted reconstitution and functional display of transgenic TCRs. a, The Jurkat E6-1 cell line was subjected to sequential CRISPR-Cas9 genome editing steps in order to generate the TnT platform. TnT cells constitutively express Cas9 and human CD8, harbor an NFAT-GFP reporter of TCR signaling, and lack expression of CD4, Fas and endogenous TCR. Reconstitution of TnT cells with transgenic TCRs via CRISPR-Cas9 HDR results in TnT-TCR cells with restored surface expression of the TCR:CD3 complex. **b**, TCR reconstitution of TnT cells targeted to the Jurkat TCRβ locus. An HDR template encoding transgenic TCRαβ chains is integrated into TnT cells via Cas9 and a gRNA targeting the endogenous Jurkat CDR3β sequence. Transgenic TCR expression is dependent on correct RNA splicing with endogenous Jurkat TRBC1. **c**, Flow cytometric assessment of CD3 restoration in TnT cells after their targeted reconstitution with TCR_{1G4} (specific for NY-ESO-1₁₅₇₋₁₆₅ peptide). **d**, Representative flow cytometry plot showing peptide-MHC dextramer binding to TnT cells (no TCR expression) and MART-1-specific TnT-TCR_{DMF5} cells. **e**, Validation of targeted TCR reconstitution in TnT-TCR_{DMF5} cells by genomic PCR of the Jurkat VDJβ region. **f**, Representative flow cytometry dot plots displaying NFAT-driven GFP expression in TnT-TCR_{1G4} cells, but not TnT cells, after overnight co-culture with T2 cells pulsed with NY-ESO-1₁₅₇₋₁₆₄ peptide. **g**, NFAT-GFP expression in TnT and TnT-TCR cells after overnight co-culture with T2 cells pulsed with NY-ESO-1₁₅₇₋₁₆₄, MART-1_{26-35(27L)} or no peptide. **h**, Serially-diluted target peptide-MHC dextramers were used to assess the binding avidities of TnT-TCR_{1G4}, TnT-TCR_{DMF4} and TnT-TCR_{DMF5} (n = 3). Peptide-MHC dextramer concentrations resulting in half-maximal proportions of dextramer positive cells (EC50) were derived from non-linear least squares fits. **i**, Normalized NFAT-GFP expression in TnT-TCR cells after overnight co-culture with T2 cells pulsed with serially-diluted cognate peptide (n = 2). Peptide pulse concentrations resulting in half-maximal proportions of NFAT-GFP+ cells (EC50) were derived from non-linear least squares fits. Data are displayed as mean ± SD.

Figure 2_Vazquez-Lombardi et al.

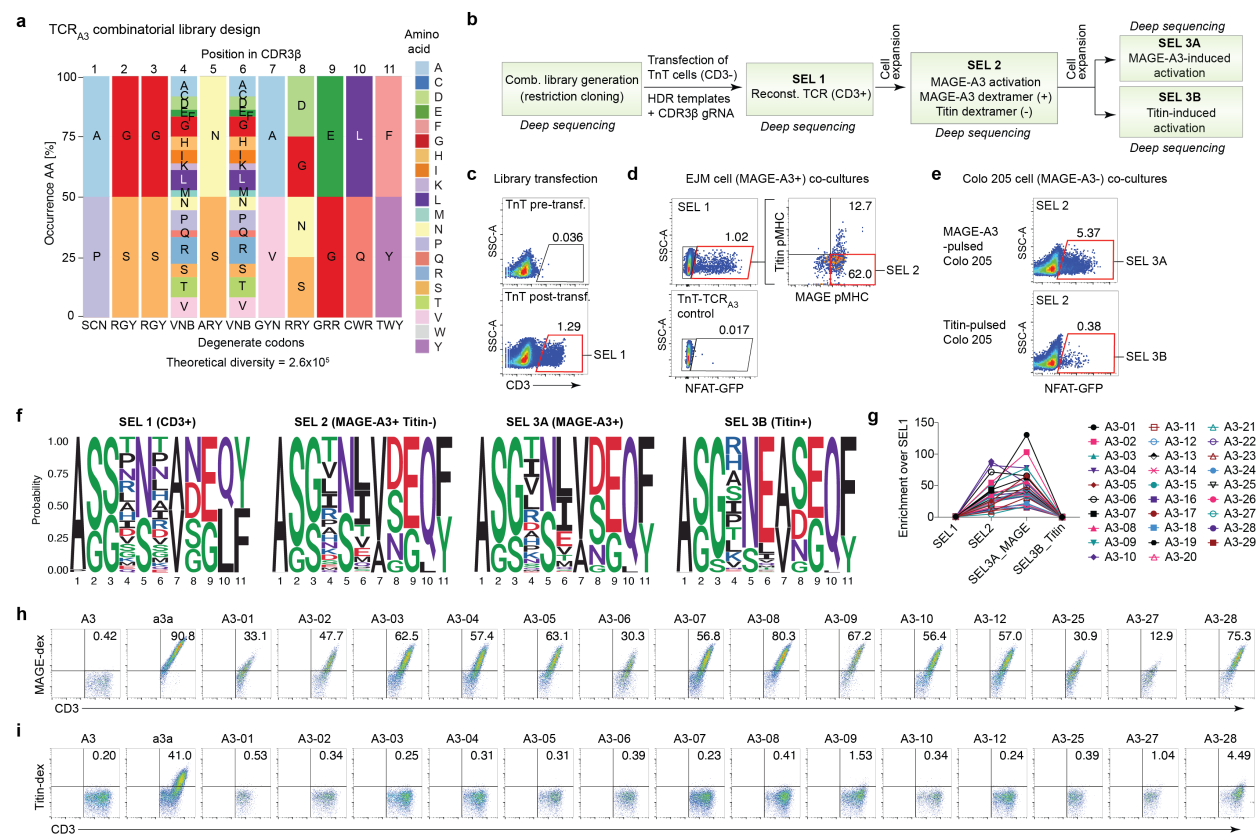


800

Figure 2. Deep mutational scanning of CDR3 β reveals the sequence landscape for TCR expression, binding and signalling. **a**, The CDR3 β sequences of TCR_{A3} and TCR_{DMF4} were subjected to deep mutational scanning (DMS). **b**, DMS libraries were generated by means of plasmid nicking saturation mutagenesis and integrated into TnT cells by Cas9 HDR. Reconstituted cells were selected by FACS based on CD3 surface expression, target peptide-MHC binding and antigen-induced signalling (co-culture with antigen-presenting cells). Deep sequencing of CDR3 β sequences was performed at every selection step. **c, d**, Heatmaps displaying the enrichment of sequencing reads from TCR_{A3} and TCR_{DMF4} variants across selections relative to their occurrence in the starting plasmid DMS libraries. Outlined boxes represent wild-type CDR3 β residues. **e-f**, Flow cytometric assessment of antigen binding and antigen-induced signalling in TnT cells reconstituted with TCR_{A3}, TCR_{a3a} and selected TCR_{A3} variants (CD3+ gate). **e**, The levels of binding to MAGE-A3 peptide-MHC dextramer (top row) and activation after overnight co-culture with MAGE-A3+ EJM cells (bottom row, proportion CD69^{high} TnT-TCR) are displayed. **f**, Graph displays the levels of antigen binding and antigen-induced signalling in TCR_{A3} single mutants relative to wild-type TCR_{A3}. **g-i**, Flow cytometric assessment of antigen binding and antigen-induced signalling in TnT cells reconstituted with TCR_{DMF4}, TCR_{DMF5} and selected TCR_{DMF4} variants (CD3+ gate). **g**, The levels of binding to MART-1 peptide-MHC dextramer (top row) and activation after overnight co-culture with MART-1-pulsed T2 cells (bottom row, proportion NFAT-GFP+ TnT-TCR) are displayed. **i**, Histograms displaying the levels of MART-1 peptide-MHC dextramer bound by TnT-TCR cells. **h**, Graph displays the levels of antigen binding and antigen-induced signalling in TCR_{DMF4} single mutants relative to wild-type TCR_{DMF4}.

Vazquez-Lombardi et al., CRISPR-targeted display and functional engineering of TCRs

Figure 3_Vazquez-Lombardi et al.

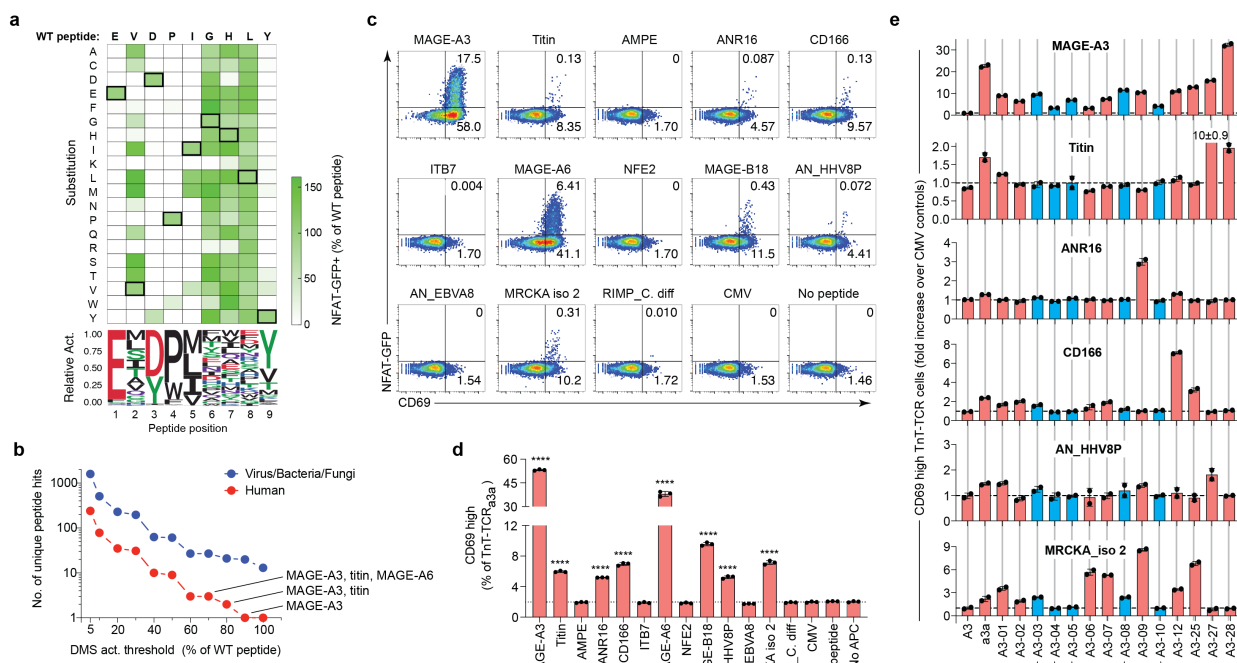


818

819

820 **Figure 3. Rational design and functional screening of combinatorial TCR mutagenesis libraries in TnT cells for**
821 **selection of enhanced target specificity.** a, Data obtained from TCR_{A3} CDR3 β DMS was utilized as input to design a
822 combinatorial mutagenesis library that has a theoretical diversity of 2.6×10^5 variants. Degenerate codons were
823 designed to recapitulate the amino acid frequencies observed in DMS selections based on MAGE-A3 peptide-MHC
824 dextramer binding and MAGE-A3-induced signalling. b, Strategy for the selection of TCR_{A3} combinatorial mutagenesis
825 variants with enhanced recognition of the MAGE-A3₁₆₈₋₁₇₆ peptide (EVDPIGHLY), while avoiding cross-reactivity to the
826 known titin_{24,337-24,345} off-target peptide (ESDPIVAQY). Deep sequencing of CDR3 β sequences was performed at every
827 selection step. c, Flow cytometry plots show selection of TCR_{A3} variants from the combinatorial library that are capable
828 of surface expression in TnT cells. TnT cells with restored CD3 surface expression were bulk-sorted (SEL 1). d, Flow
829 cytometry plots showing TnT-TCR cells (from SEL 1) with positive MAGE-A3-induced signalling (NFAT-GFP+), positive
830 MAGE-A3 peptide-MHC binding and negative titin peptide-MHC binding; cells were bulk-sorted (SEL 2) and expanded
831 in culture. e, Expanded SEL 2 cells were co-cultured overnight with either MAGE-A3 peptide-pulsed or titin peptide-
832 pulsed Colo 205 cells and bulk-sorted for activation by NFAT-GFP+ expression (SEL 3A and SEL 3B). f, Amino acid
833 sequence logos showing the frequency of specific residues at each CDR3 β position across selections (logos weighted
834 on unique clone frequencies). g, TCR_{A3} variants with predicted high specificity for MAGE-A3 and their enrichment across
835 selections based on deep sequencing data. h-i, Flow cytometry plots of TnT cells reconstituted with TCR_{A3}, TCR_{a3a} and
836 selected TCR_{A3} combinatorial variants. Cells were assessed for CD3 expression, MAGE-A3 peptide-MHC binding (h)
837 and titin peptide-MHC binding (i). Cells in the CD3+ gate are shown. Degenerate nucleotide symbols: R = A, G; Y = C,
838 T; S = G, C; W = A, T; K = G, T; M = A, C; B = C, G, T; D = A, G, T; H = A, C, T; V = A, C, G; N = any base.

Figure 4_Vazquez-Lombardi et al.



840

841 **Figure 4. The TnT platform enables TCR cross-reactivity profiling and prediction of off-target peptides.** . a, The
842 cross-reactivity profile of TnT-TCR_{α3a} cells was assessed using single mutant variants of the wild-type MAGE-A3 peptide
843 (peptide DMS library), which were pulsed on Colo 205 cells for individual co-culture assays (n = 171). Heatmap shows
844 the proportion of NFAT-GFP+ TnT-TCR_{α3a} cells after co-culture, as determined by flow cytometry. Data are normalized
845 to the response induced by the MAGE-A3 wild-type peptide (boxed residues). Sequence logo shows the relative activity
846 of peptide DMS library members carrying mutations at the same peptide position. b, The sequences of peptides
847 mediating 5, 10, 20, 30, 40, 50, 60, 70, 80, 90 and 100 percent activation relative to the MAGE-A3 wild-type peptide
848 were utilized to generate motifs to query the UniProtKB database. Dot plot displays the number of human (red) and non-
849 human (blue) unique peptide hits resulting from these searches. The first (MAGE-A3), second (titin) and third (MAGE-
850 A6) highest predicted activating peptides are highlighted. c, Flow cytometry of CD69 and NFAT-GFP expression
851 following co-culture with peptide-pulsed Colo 205 cells shows cross-reactivity of TnT-TCR_{α3a} cells against a subset of
852 predicted off-target peptides. The CMV peptide (HLA-A*0101-restricted, VTEHDTLLY) is included as a negative control.
853 d, Bar graph shows repeat of the experiment in (c) performed in triplicate. The percentages of CD69^{high} TnT-TCR_{α3a}
854 cells after co-culture with peptide-pulsed Colo 205 cells were utilized to assess reactivity to each peptide. Dotted line
855 reflects the mean of CMV-pulsed controls (Y = 1.98). Asterisks indicate significant differences to CMV controls as
856 determined by two-way ANOVA with Bonferroni post-hoc test for multiple comparisons. e, Assessment of selected TnT-
857 TCR_{α3} CDR3β variants for cross-reactivity. TnT cells expressing TCR_{α3}, TCR_{α3a} and selected TnT_{α3} variants were
858 co-cultured with Colo 205 cells pulsed with a subset of predicted off-target peptides. The percentages of CD69^{high} TnT-
859 TCR cells were determined by flow cytometry and normalized to their respective CMV backgrounds (n = 2). Selected
860 TnT-TCR_{α3} variants displaying favorable cross-reactivity profiles are highlighted in blue. Data are displayed as mean ±
861 SD. * P < 0.05, ** P < 0.01, *** P < 0.001, **** P < 0.0001, ns = not significant. See Supplementary Table 5 for a full list
862 of peptides and their sequences.

863

864

865

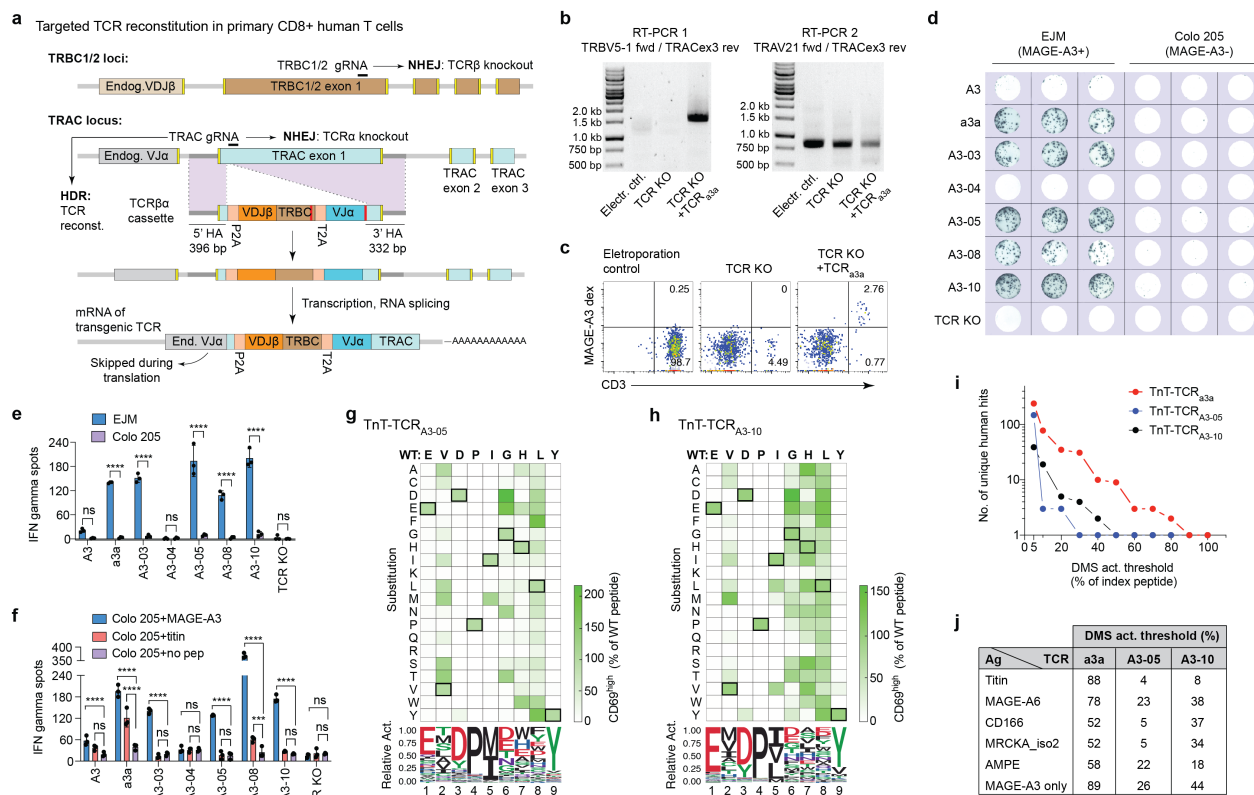
866

867

868

869

Figure 5_Vazquez-Lombardi et al.



870

Figure 5. The TnT platform and primary T cells validate the engineering of TCRs with enhanced target reactivity and minimal cross-reactivity. **a**, Schematic shows TCR reconstitution in primary human CD8+ T cells is targeted to the TRAC locus by Cas9 HDR. T cells were transfected with TRAC and TRBC1/2 gRNAs in complex with recombinant Cas9 for dual knockout of endogenous TCR α and TCR β chains. TCR β cassette consisted of a P2A self-processing peptide, followed by VDJ β and TRBC domains, a T2A self-processing peptide and a VJ α domain. Regions highlighted in red were re-coded in order to prevent targeting of HDR templates. Transgenic TCR expression is dependent on correct RNA splicing with endogenous TRAC exons 2 and 3. **b**, Validation of targeted TCR $_{a3a}$ integration by means of RT-PCR with a forward primer annealing to the transgenic TRBV5-1 gene and a reverse primer annealing to the endogenous TRAC exon 3. Electroporation control and dual TCR knockout samples display no PCR product, while samples derived from TCR $_{a3a}$ transfectants display a 1.6 kb product consistent with targeted TCR integration and correct splicing with endogenous TRAC. A second RT-PCR reaction amplifying both endogenous and transgenic TRAV21-TRAC sequences was included as a positive control. **c**, Flow cytometric assessment of CD3 expression and MAGE-A3 peptide-MHC dextramer binding in primary CD8+ T cells reconstituted with TCR $_{a3a}$. **d**, IFN- γ ELISPOT assays for assessment of primary CD8+ T cells reconstituted with selected TCRs following co-culture with MAGE-A3-positive EJM cells or MAGE-A3-negative Colo 205 cells (n = 3; 5x10⁴ T cells per well). **e**, Quantification of IFN- γ ELISpot data in **d**. Asterisks indicate significant differences as determined by two-way ANOVA with Bonferroni post-hoc test for multiple comparisons. **f**, Quantification of IFN- γ ELISpot data from primary CD8+ T cells reconstituted with selected TCRs following overnight co-culture with Colo 205 cells pulsed with MAGE-A3₁₆₈₋₁₇₆, titin_{24,337-24,345}, or no peptide (n = 3; 4x10⁵ T cells per well). Asterisks indicate significant differences to non-pulsed Colo 205 controls as determined by two-way ANOVA with Bonferroni post hoc test for multiple comparisons. **g, h**, The cross-reactivity profiles of TnT-TCR $_{A3-05}$ and TnT-TCR $_{A3-10}$ cells were assessed by individual co-cultures with Colo 205 cells pulsed with single mutant variants (DMS library) of the wild-type MAGE-A3₁₆₈₋₁₇₆ peptide (n = 171 variants). Heatmaps represent the proportions of CD69^{high} TnT-TCR cells after overnight co-culture, as determined by flow cytometry. Data are normalized to the response induced by wild-type peptide (boxed residues). Sequence logos show the relative activity of peptide DMS library members carrying mutations at the same peptide position. **i**, The sequences of peptides mediating 5, 10, 20, 30, 40, 50, 60, 70, 80, 90 and 100 percent activation relative to wild-type peptide were utilized to generate motifs to query the UniProtKB database. Dot plots display the number of unique human activating peptides resulting from these searches. The TnT-TCR $_{a3a}$ cross-reactivity profile is displayed for comparison purposes. **j**, Comparison of the highest activation thresholds at which peptide DMS motifs derived from TnT-TCR $_{a3a}$, TnT-TCR $_{A3-05}$ and TnT-TCR $_{A3-10}$ return off-target peptides: titin, MAGE-A6, CD166, MRCKA isoform 2 or glutamyl aminopeptidase (AMPE). The lowest activation threshold at which MAGE-A3 peptide becomes the only predicted activating antigen is also displayed. Data are displayed as mean \pm SD; * P < 0.05, ** P < 0.01, *** P < 0.001, **** P < 0.0001, ns = not significant.

903 **References**

- 904 1. Schmitt, T. M., Ragnarsson, G. B. & Greenberg, P. D. T cell receptor gene therapy for cancer. *Hum. Gene Ther.*
905 **20**, 1240–1248 (2009).
- 906 2. Garber, K. Driving T-cell immunotherapy to solid tumors. *Nat. Biotechnol.* **36**, 215–219 (2018).
- 907 3. Newick, K., Moon, E. & Albelda, S. M. Chimeric antigen receptor T-cell therapy for solid tumors. *Molecular*
908 *Therapy - Oncolytics* vol. 3 16006 (2016).
- 909 4. Zhang, J. & Wang, L. The Emerging World of TCR-T Cell Trials Against Cancer: A Systematic Review.
910 *Technology in Cancer Research & Treatment* vol. 18 153303381983106 (2019).
- 911 5. Rapoport, A. P. et al. NY-ESO-1-specific TCR-engineered T cells mediate sustained antigen-specific antitumor
912 effects in myeloma. *Nat. Med.* **21**, 914–921 (2015).
- 913 6. Morgan, R. A. et al. Cancer Regression and Neurological Toxicity Following Anti-MAGE-A3 TCR Gene Therapy.
914 *Journal of Immunotherapy* vol. 36 133–151 (2013).
- 915 7. Johnson, L. A. et al. Gene therapy with human and mouse T-cell receptors mediates cancer regression and
916 targets normal tissues expressing cognate antigen. *Blood* **114**, 535–546 (2009).
- 917 8. Morgan, R. A. et al. Cancer regression in patients after transfer of genetically engineered lymphocytes. *Science*
918 **314**, 126–129 (2006).
- 919 9. Robbins, P. F. et al. A pilot trial using lymphocytes genetically engineered with an NY-ESO-1-reactive T-cell
920 receptor: long-term follow-up and correlates with response. *Clin. Cancer Res.* **21**, 1019–1027 (2015).
- 921 10. Parkhurst, M. R. et al. T cells targeting carcinoembryonic antigen can mediate regression of metastatic colorectal
922 cancer but induce severe transient colitis. *Mol. Ther.* **19**, 620–626 (2011).
- 923 11. Klebanoff, C. A., Rosenberg, S. A. & Restifo, N. P. Prospects for gene-engineered T cell immunotherapy for solid
924 cancers. *Nat. Med.* **22**, 26–36 (2016).
- 925 12. Strønen, E. et al. Targeting of cancer neoantigens with donor-derived T cell receptor repertoires. *Science* **352**,
926 1337–1341 (2016).
- 927 13. Uttenhal, B. J., Chua, I., Morris, E. C. & Stauss, H. J. Challenges in T cell receptor gene therapy. *The Journal of*
928 *Gene Medicine* vol. 14 386–399 (2012).
- 929 14. Linette, G. P. et al. Cardiovascular toxicity and titin cross-reactivity of affinity-enhanced T cells in myeloma and
930 melanoma. *Blood* **122**, 863–871 (2013).
- 931 15. Sewell, A. K. Why must T cells be cross-reactive? *Nat. Rev. Immunol.* **12**, 669–677 (2012).
- 932 16. Bentzen, A. K. et al. T cell receptor fingerprinting enables in-depth characterization of the interactions governing
933 recognition of peptide-MHC complexes. *Nat. Biotechnol.* (2018) doi:10.1038/nbt.4303.
- 934 17. Wooldridge, L. et al. A single autoimmune T cell receptor recognizes more than a million different peptides. *J.*
935 *Biol. Chem.* **287**, 1168–1177 (2012).
- 936 18. Sibener, L. V. et al. Isolation of a Structural Mechanism for Uncoupling T Cell Receptor Signaling from Peptide-
937 MHC Binding. *Cell* **174**, 672–687.e27 (2018).
- 938 19. Hebeisen, M. et al. Identifying Individual T Cell Receptors of Optimal Avidity for Tumor Antigens. *Front. Immunol.*
939 **6**, 582 (2015).
- 940 20. Presotto, D. et al. Fine-Tuning of Optimal TCR Signaling in Tumor-Redirected CD8 T Cells by Distinct TCR
941 Affinity-Mediated Mechanisms. *Front. Immunol.* **8**, 1564 (2017).
- 942 21. Hebeisen, M. et al. SHP-1 phosphatase activity counteracts increased T cell receptor affinity. *J. Clin. Invest.* **123**,
943 1044–1056 (2013).
- 944 22. Thomas, S. et al. Human T cells expressing affinity-matured TCR display accelerated responses but fail to
945 recognize low density of MHC-peptide antigen. *Blood* vol. 118 319–329 (2011).
- 946 23. Tan, M. P. et al. T cell receptor binding affinity governs the functional profile of cancer-specific CD8+ T cells. *Clin.*
947 *Exp. Immunol.* **180**, 255–270 (2015).
- 948 24. Duong, M. N., Erdes, E., Hebeisen, M. & Rufer, N. Chronic TCR-MHC (self)-interactions limit the functional
949 potential of TCR affinity-increased CD8 T lymphocytes. *J Immunother Cancer* **7**, 284 (2019).
- 950 25. Spindler, M. J. et al. Massively parallel interrogation and mining of natively paired human TCR β repertoires.
951 *Nat. Biotechnol.* **38**, 609–619 (2020).
- 952 26. Johnson, L. A. et al. Gene transfer of tumor-reactive TCR confers both high avidity and tumor reactivity to
953 nonreactive peripheral blood mononuclear cells and tumor-infiltrating lymphocytes. *J. Immunol.* **177**, 6548–6559
954 (2006).
- 955 27. Chapuis, A. G. et al. T cell receptor gene therapy targeting WT1 prevents acute myeloid leukemia relapse post-
956 transplant. *Nat. Med.* **25**, 1064–1072 (2019).
- 957 28. Kieke, M. C. et al. Selection of functional T cell receptor mutants from a yeast surface-display library. *Proc. Natl.*
958 *Acad. Sci. U. S. A.* **96**, 5651–5656 (1999).
- 959 29. Li, Y. et al. Directed evolution of human T-cell receptors with picomolar affinities by phage display. *Nat.*
960 *Biotechnol.* **23**, 349–354 (2005).
- 961 30. Cameron, B. J. et al. Identification of a Titin-derived HLA-A1-presented peptide as a cross-reactive target for

962 engineered MAGE A3-directed T cells. *Sci. Transl. Med.* **5**, 197ra103 (2013).

963 31. Karapetyan, A. R. *et al.* TCR Fingerprinting and Off-Target Peptide Identification. *Front. Immunol.* **10**, 2501
964 (2019).

965 32. Malecek, K. *et al.* Engineering improved T cell receptors using an alanine-scan guided T cell display selection
966 system. *J. Immunol. Methods* **392**, 1–11 (2013).

967 33. Wagner, E. K. *et al.* Human cytomegalovirus-specific T-cell receptor engineered for high affinity and soluble
968 expression using mammalian cell display. *J. Biol. Chem.* **294**, 5790–5804 (2019).

969 34. Chervin, A. S., Aggen, D. H., Raseman, J. M. & Kranz, D. M. Engineering higher affinity T cell receptors using a
970 T cell display system. *Journal of Immunological Methods* vol. 339 175–184 (2008).

971 35. Kessels, H. W., van Den Boom, M. D., Spits, H., Hooijberg, E. & Schumacher, T. N. Changing T cell specificity by
972 retroviral T cell receptor display. *Proc. Natl. Acad. Sci. U. S. A.* **97**, 14578–14583 (2000).

973 36. Schmitt, T. M. *et al.* Generation of higher affinity T cell receptors by antigen-driven differentiation of progenitor T
974 cells in vitro. *Nat. Biotechnol.* **35**, 1188–1195 (2017).

975 37. Bentzen, A. K. *et al.* Large-scale detection of antigen-specific T cells using peptide-MHC-I multimers labeled with
976 DNA barcodes. *Nat. Biotechnol.* **34**, 1037–1045 (2016).

977 38. Zhang, S.-Q. *et al.* High-throughput determination of the antigen specificities of T cell receptors in single cells.
978 *Nature Biotechnology* vol. 36 1156–1159 (2018).

979 39. Gee, M. H. *et al.* Antigen Identification for Orphan T Cell Receptors Expressed on Tumor-Infiltrating
980 Lymphocytes. *Cell* **172**, 549–563.e16 (2018).

981 40. Gee, M. H., Yang, X. & Christopher Garcia, K. Facile method for screening clinical T cell receptors for off-target
982 peptide-HLA reactivity. doi:10.1101/472480.

983 41. Birnbaum, M. E. *et al.* Deconstructing the peptide-MHC specificity of T cell recognition. *Cell* **157**, 1073–1087
984 (2014).

985 42. Rius, C. *et al.* Peptide–MHC Class I Tetramers Can Fail To Detect Relevant Functional T Cell Clonotypes and
986 Underestimate Antigen-Reactive T Cell Populations. *The Journal of Immunology* vol. 200 2263–2279 (2018).

987 43. Joglekar, A. V. *et al.* T cell antigen discovery via signaling and antigen-presenting bifunctional receptors. *Nat.*
988 *Methods* **16**, 191–198 (2019).

989 44. Kisielow, J., Obermair, F.-J. & Kopf, M. Deciphering CD4 T cell specificity using novel MHC-TCR chimeric
990 receptors. *Nat. Immunol.* **20**, 652–662 (2019).

991 45. Li, G. *et al.* T cell antigen discovery via trogocytosis. *Nat. Methods* **16**, 183–190 (2019).

992 46. Sharma, G., Rive, C. M. & Holt, R. A. Rapid selection and identification of functional CD8 T cell epitopes from
993 large peptide-coding libraries. *Nat. Commun.* **10**, 4553 (2019).

994 47. Kula, T. *et al.* T-Scan: A Genome-wide Method for the Systematic Discovery of T Cell Epitopes. *Cell* **178**, 1016–
995 1028.e13 (2019).

996 48. Border, E. C., Sanderson, J. P., Weissensteiner, T., Gerry, A. B. & Pumphrey, N. J. Affinity-enhanced T-cell
997 receptors for adoptive T-cell therapy targeting MAGE-A10: strategy for selection of an optimal candidate.
998 *Oncoimmunology* **8**, e1532759 (2019).

999 49. Sanderson, J. P. *et al.* Preclinical evaluation of an affinity-enhanced MAGE-A4-specific T-cell receptor for
1000 adoptive T-cell therapy. *Oncoimmunology* **9**, 1682381 (2020).

1001 50. Sather, B. D. *et al.* Efficient modification of CCR5 in primary human hematopoietic cells using a megaTAL
1002 nuclease and AAV donor template. *Sci. Transl. Med.* **7**, 307ra156 (2015).

1003 51. Mason, D. M. *et al.* High-throughput antibody engineering in mammalian cells by CRISPR/Cas9-mediated
1004 homology-directed mutagenesis. *Nucleic Acids Res.* **46**, 7436–7449 (2018).

1005 52. Hockemeyer, D. *et al.* Efficient targeting of expressed and silent genes in human ESCs and iPSCs using zinc-
1006 finger nucleases. *Nat. Biotechnol.* **27**, 851–857 (2009).

1007 53. Robbins, P. F. *et al.* Single and dual amino acid substitutions in TCR CDRs can enhance antigen-specific T cell
1008 functions. *J. Immunol.* **180**, 6116–6131 (2008).

1009 54. Luft, T. *et al.* Exogenous peptides presented by transporter associated with antigen processing (TAP)-deficient
1010 and TAP-competent cells: intracellular loading and kinetics of presentation. *J. Immunol.* **167**, 2529–2537 (2001).

1011 55. Borbulevych, O. Y., Santhanagopalan, S. M., Hossain, M. & Baker, B. M. TCRs used in cancer gene therapy
1012 cross-react with MART-1/Melan-A tumor antigens via distinct mechanisms. *J. Immunol.* **187**, 2453–2463 (2011).

1013 56. Schober, K. *et al.* Orthotopic replacement of T-cell receptor α - and β -chains with preservation of near-
1014 physiological T-cell function. *Nat Biomed Eng* **3**, 974–984 (2019).

1015 57. Karanikas, V. *et al.* Monoclonal anti-MAGE-3 CTL responses in melanoma patients displaying tumor regression
1016 after vaccination with a recombinant canarypox virus. *J. Immunol.* **171**, 4898–4904 (2003).

1017 58. Connerette, T. *et al.* Functions of Anti-MAGE T-cells induced in melanoma patients under different vaccination
1018 modalities. *Cancer Res.* **68**, 3931–3940 (2008).

1019 59. Wrenbeck, E. E. *et al.* Plasmid-based one-pot saturation mutagenesis. *Nat. Methods* **13**, 928–930 (2016).

1020 60. Weon, J. L. & Potts, P. R. The MAGE protein family and cancer. *Current Opinion in Cell Biology* vol. 37 1–8
1021 (2015).

Vazquez-Lombardi et al., CRISPR-targeted display and functional engineering of TCRs

1022 61. Roth, T. L. *et al.* Reprogramming human T cell function and specificity with non-viral genome targeting. *Nature*
1023 **559**, 405–409 (2018).

1024 62. Ren, J. *et al.* A versatile system for rapid multiplex genome-edited CAR T cell generation. *Oncotarget* **8**, 17002–
1025 17011 (2017).

1026 63. Raman, M. C. C. *et al.* Direct molecular mimicry enables off-target cardiovascular toxicity by an enhanced affinity
1027 TCR designed for cancer immunotherapy. *Sci. Rep.* **6**, 18851 (2016).

1028 64. Zhao, Y. *et al.* Cloning and chromosomal location of a novel member of the myotonic dystrophy family of protein
1029 kinases. *J. Biol. Chem.* **272**, 10013–10020 (1997).

1030 65. Picelli, S. *et al.* Full-length RNA-seq from single cells using Smart-seq2. *Nat. Protoc.* **9**, 171–181 (2014).

1031 66. Wagih, O. ggseqlogo: a versatile R package for drawing sequence logos. *Bioinformatics* vol. 33 3645–3647
1032 (2017).